

Adana Alparslan Türkeş Bilim ve Teknoloji Üniversitesi

BİLİM DERGİSİ



ATU

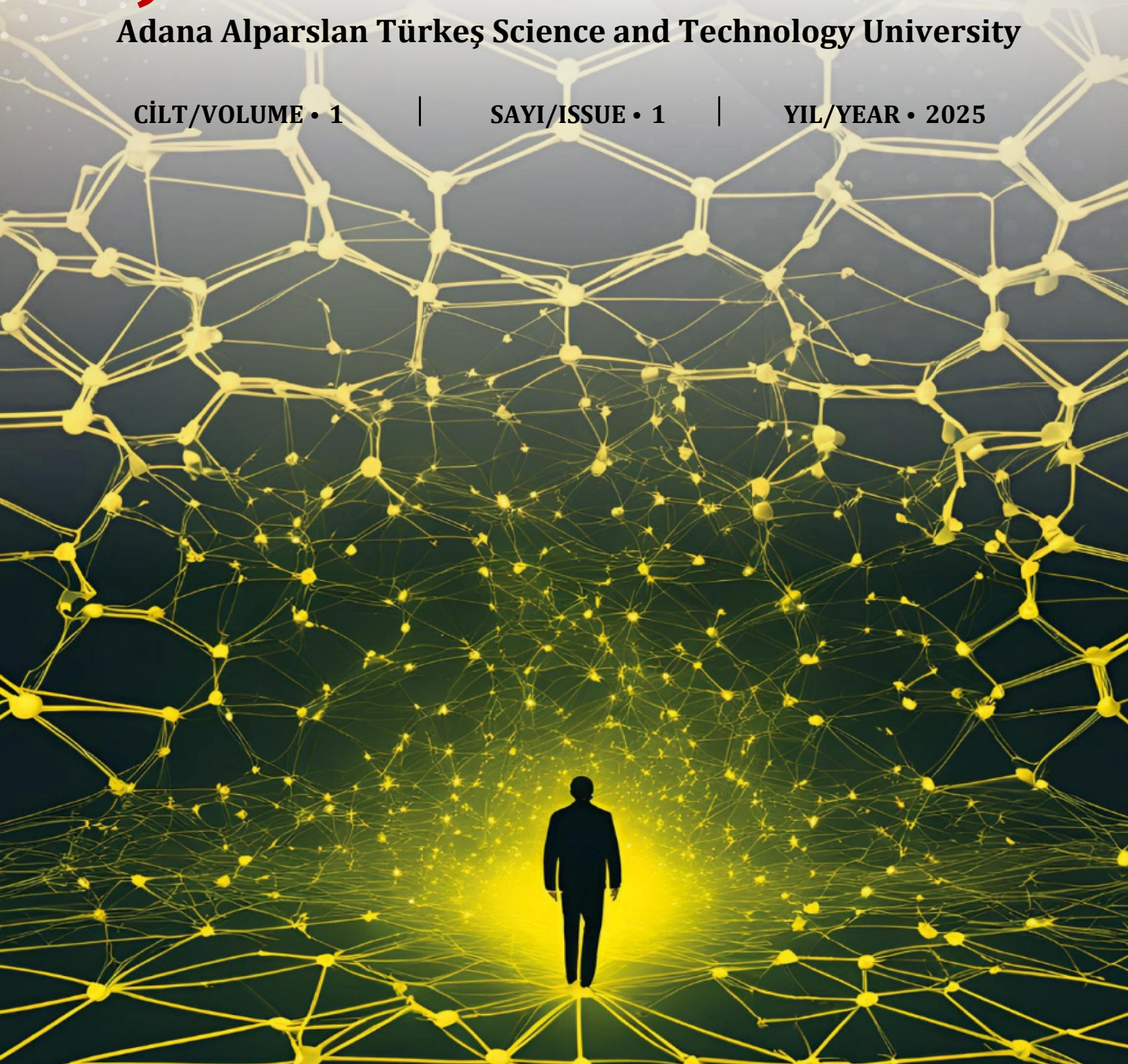
JOURNAL OF SCIENCE

Adana Alparslan Türkeş Science and Technology University

CİLT/VOLUME • 1

SAYI/ISSUE • 1

YIL/YEAR • 2025



Dergi Adı
Adana Alparslan Türkeş Bilim ve Teknoloji
Üniversitesi Bilim Dergisi

Journal Name
Adana Alparslan Türkeş Science and Technology
University Journal of Science

Yayımcı
Adana Alparslan Türkeş Bilim ve Teknoloji
Üniversitesi

Publisher
Adana Alparslan Türkeş Science and Technology
University

Yayımlama Periyodu
Yılda iki kez (Haziran ve Aralık)

Publication Period
Published twice a year (June and December)

Yayın Dili
Türkçe veya İngilizce

Publication Language
Turkish or English

Yayın Değerlendirme
Hakemli (kör)

Publication Reviewing Process
Peer-reviewed (blind)

Yayın Politikası
Açık kaynak (ücretsiz)

Publication Policy
Open access (free)

Dergi Hakkında

Adana Alparslan Türkeş Bilim ve Teknoloji Bilim Dergisi mühendislik ve fen bilimleri konularını kapsayan bir dergidir. ATÜ Bilim Dergisi, ulusal ve uluslararası düzeyde bilim, mühendislik ve teknoloji alanlarında özgün araştırma makalelerini veya ilgili alandaki bilimsel makaleleri yeterli sayıda tarayıp konuyu bugünkü bilgi düzeyinde özetleyen ve deneysel/teorik bulguları karşılaştırarak yorumlayan tarama makalelerini kabul etmektedir.

About the Journal

Adana Alparslan Türkeş Science and Technology Journal of Science is a journal covering engineering and science subjects. ATÜ Science Journal accepts original research articles in the fields of science, engineering and technology at national and international levels or review articles that scan a sufficient number of scientific articles in the relevant field, summarize the subject at the current level of knowledge and compare and interpret experimental/theoretical findings.

Dergi Adı Kısaltması

ATU Bilim Dergisi

Journal Title Abbreviation

ATU Journal of Science

Dergi Sahibi

Prof. Dr. Adnan Sözen
(Rektör/Rector)

Journal Owner

Baş Editör

Prof. Dr. Mustafa Akyol

Editor in Chief

Editör Yardımcısı

Prof. Dr. Erinc Uludamar

Deputy Editor

Alan Editörleri

Section Editors

Prof. Dr. Ahmet Ekicibil	Çukurova University, Türkiye	Material Physics, Electronic and Magnetic Properties of Condensed Matter; Superconductivity
Prof. Dr. M. Yusuf Tanrıkulu	Adana Alparslan Türkeş Science and Technology University, Türkiye	Photonic and Electro-Optical Devices, Sensors and Systems, Microelectronics, Microelectromechanical Systems (MEMS)
Prof. Dr. Salih Yılmaz	Adana Alparslan Türkeş Science and Technology University, Türkiye	Material Physics, Photovoltaic Devices (Solar Cells), Semiconductors
Prof. Dr. Ahmet Beycioglu	Adana Alparslan Türkeş Science and Technology University, Türkiye	Construction Materials, Production Technologies
Prof. Dr. Haluk Koralay	Gazi University, Türkiye	General Physics, Electronic and Magnetic Properties of Condensed Matter; Superconductivity
Prof. Dr. Tayfun Yusuf Yünsel	Adana Alparslan Türkeş Science and Technology University, Türkiye	Mining Engineering
Prof. Dr. Zafer Erbay	Adana Alparslan Türkeş Science and Technology University, Türkiye	Food Packaging, Preservation and Processing, Food Sustainability
Assoc. Prof. Dr. Müslüm Demir	Boğaziçi University, Türkiye	Electrochemistry, Wastewater Treatment Processes, Electrochemical Technologies
Assoc. Prof. Dr. Ali İnan	Adana Alparslan Türkeş Science and Technology University, Türkiye	Information Security and Cryptology
Assoc. Prof. Dr. Yeliz Gurdal	Adana Alparslan Türkeş Science and Technology University, Türkiye	Catalysis and Mechanisms of Reactions, Theoretical and Computational Chemistry
Assoc. Prof. Dr. Gökay Dışken	Adana Alparslan Türkeş Science and Technology University, Türkiye	Signal Processing
Assoc. Prof. Dr. Yelda Durgun Şahin	Adana Alparslan Türkeş Science and Technology University, Türkiye	Urban History, Transport Planning, Architectural Design, Universal and Unobstructed Design
Assoc. Prof. Dr. Mehmet Ali Olğar	Niğde Ömer Halisdemir University, Türkiye	Physics Education, Condensed Matter Characterization Technique Development
Assoc. Prof. Dr. Tahir Durhasan	Adana Alparslan Türkeş Science and Technology University, Türkiye	Fluid Mechanics and Thermal Engineering, Aerodynamics, Computational Methods in Fluid Flow
Assist. Prof. Dr. Erdi Tosun	Çukurova University, Türkiye	Renewable Energy Resources , Internal Combustion Engines, Automotive Combustion and Fuel Engineering

Dil Editörleri

Language Editors

Assoc.Prof. Dr. Duygu İşpınar Akçayoğlu
Res.Asst. Beyza Betül Tanrıkulu
Dr. Hilal Gülben Gerek
Gözde Salur

Yayın Etiği Kurulu

Publication Ethics Board

Prof. Dr. Başak Doğru Mert
Prof. Dr. Gökhan Tüccar

Sekreter

Secretary

Res. Asst. Ümit Kılıç

Teknik Sorumlu

Technical Support

Burak Somuncu

Danışma Kurulu

Advisory Board

Prof. Dr. Serkan Selli	Çukurova University, Türkiye
Prof. Dr. Haşim Kelebek	Adana Alparslan Türkeş Science and Technology University, Türkiye
Prof. Dr. Recep Zan	Niğde Ömer Halisdemir University, Türkiye
Prof. Dr. Muharrem Karaaslan	İskenderun Technical University, Türkiye
Prof. Dr. Mustafa Çam	Erciyes University, Türkiye
Prof. Dr. Hakan Ateş	Gazi University, Türkiye
Prof. Dr. Çetin Karataş	Gazi University, Türkiye
Prof. Dr. Murat Hoşöz	Kocaeli University, Türkiye
Assoc. Prof. Dr. Battal Doğan	Gazi University, Türkiye
Assoc. Prof. Dr. Adem Tekerek	Gazi University, Türkiye
Assoc. Prof. Dr. Zeynep Aytaç	Gazi University, Türkiye

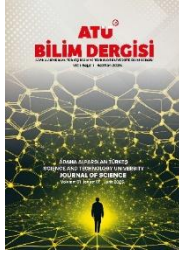
İletişim

Contact

ATU Bilim Dergisi Editörlüğü
Adana Alparslan Türkeş Bilim ve Teknoloji Üniversitesi
Lisansüstü Eğitim Enstitüsü
01250 Sarıçam
ADANA –TÜRKİYE
Tel : 0322-455 00 00
Fax : 0322-455 00 02
atubd@atu.edu.tr
www.dergipark.com/atujscience

İÇİNDEKİLER / CONTENTS

Araştırma Makalesi / Research Articles		Sayfa No / Page Number
1	A strategy for enhancing the performance of CdS-based hybrid photovoltaic cells via Co addition Salih Yılmaz, Murat Tomakin, Emin Bacaksız	1-8
2	Seasonal analysis of solar energy and hydrogen production potential in Adana Başak Doğru Mert, Hüseyin Nazlıgöl, Mehmet Erman Mert	9-18
3	Green synthesis of ZnO nanoparticles using pine bark extract Faruk Aslan, Ahmet Ekicibil	19-27
4	Efficiency analysis of clutch production line stations in the automotive industry using multi-criteria decision-making methods Adnan Abdulvahitoğlu, Aslı Abdulvahitoğlu, İrem Salman	28-39
5	Determination of changes in antioxidant potential of different plant infusions during storage Levent Yurdaer Aydemir, Fatma Gizem Akçakaya	40-49



A strategy for enhancing the performance of CdS-based hybrid photovoltaic cells via Co addition

Salih Yılmaz^{1,*}, Murat Tomakin², Emin Bacaksız³

¹Adana Alparslan Türkeş Science and Technology University, Department of Materials Science and Engineering, 01250 Adana, Türkiye

ORCID: 0000-0002-3006-4473

²Recep Tayyip Erdoğan University, Department of Physics, 53100 Rize, Türkiye

ORCID: 0000-0003-1887-848X

³Karadeniz Technical University, Department of Physics, 61080 Trabzon, Türkiye

ORCID: 0000-0002-0041-273X

#Corresponding Author:

E-mail: salihiyilmaz@atu.edu.tr

Abstract

This paper demonstrates the positive role of Co atoms on the performance of CdS-based hybrid photovoltaics. Spherical shaped CdS and CdS:Co films were grown on indium tin oxide (ITO)-covered glass slides, while P3HT was individually covered on these spheres. The transparency of devices improved with introducing the Co atoms into CdS matrix in the near infrared region, while a corresponding reduction in absorption was noted. Photoluminescence (PL) data showed that a diminish in the peak intensity of PL, suggesting the development of additional defect levels in the band gap which behaves as non-radiative recombination centers. The current density-voltage (J-V) characteristics indicated that the ITO/N719/CdS:Co(5%)/P3HT/Ag device achieved an overall efficiency of 0.028%, representing almost a sixfold increase over the control device. This enhancement is possibly attributed to the enhanced generation of electron-hole pairs owing to effective charge separation at the CdS:Co/P3HT interface.

Keywords: CdS:Co thin films; P3HT; CBD; optical properties; power conversion efficiency

CdS tabanlı hibrit fotovoltaiik hücrelerin performansını Co ekleme yoluyla iyileştirmeye yönelik bir strateji

Öz

Bu makale, CdS tabanlı hibrit güneş hücrelerinin performansında Co atomlarının olumlu rolünü ortaya koymaktadır. Küresel şekilli CdS ve CdS:Co filmler indiyum kalay oksit (ITO) kaplı cam plakalar üzerine büyütülmüş ve bu kürecikler üzerine P3HT'nin bireysel olarak kaplandığı görülmüştür. Cihazların geçirgenliği, CdS matrisine Co atomlarının ilave edilmesiyle yakın kızılötesi bölgede artış gösterirken, buna karşılık gelen bir absorpsiyon azalması gözlemlenmiştir. Fotoluminesans (PL) verileri, PL pik şiddetinde bir düşüş olduğunu ve bu durumun, bant aralığında radyatif olmayan rekombinasyon merkezleri olarak işlev gören ek kusur seviyelerinin oluşumuna işaret ettiğini göstermiştir. Akım yoğunluğu-gerilim (J-V) karakteristikleri, ITO/N719/CdS:Co(5%)/P3HT/Ag cihazının %0,028'lik bir toplam verimlilik elde ettiğini ve bu verimliliğin referans cihazına kıyasla yaklaşık altı kat artış sağladığını göstermiştir. Bu iyileşmenin, CdS:Co/P3HT ara yüzündeki etkin yük ayrımı sayesinde artan elektron-delik çiftlerinin oluşumuna atfedilmektedir.

Anahtar Kelimeler: CdS:Co ince filmler; P3HT; KBÇ; optik özellikler; güç dönüşüm verimliliği

Received: 4/12/2024

Revised: 25/12/2024

Accepted: 3/01/2025

Online Published: 20/06/2025

How to Cite: Yılmaz S., Tomakin M., Bacaksız E. "A strategy for enhancing the performance of CdS-based hybrid photovoltaic cells via Co addition" Adana Alparslan Türkeş Science and Technology University Journal of Science, **1** (1): 1-8 (2025).

1. Introduction

In recent years, interest in CdS-based optoelectronic devices has increased due to the advantageous properties of CdS, including its high absorption coefficient, high transmittance, low resistivity, n-type conductivity, and favorable band gap of 2.42 eV at 300 K [1]. These optical and electrical properties make CdS an excellent candidate for applications in photodetectors [2], gas sensors [3], light-emitting diodes (LEDs) [4], and solar cells [5]. In addition to traditional inorganic solar cells, CdS has also been employed as an inorganic component in hybrid solar cells, where it forms a heterostructure with an organic layer. This type of solar cell combines the advantageous properties of both inorganic and organic materials in a single device, leveraging the strengths of each. Specifically, P3HT is commonly employed as the organic layer due to its strong absorption in the visible region, moderate band gap (1.90 eV), good conductivity and hole mobility, flexibility, and compatibility with blends [6].

A good strategy for improving material properties is doping with an appropriate element. For this purpose, Co was chosen due to its abundance and non-toxicity. Previous studies showed that incorporating Co atoms into CdS created additional energy states within the band gap, which enhanced efficiency [7]. Furthermore, Co-doping may lead to more transparent CdS thin films by reducing optical losses [8]. According to our literature review, there is growing interest in studies on CdS-based heterostructures with a focus on photovoltaic characteristics. For instance, Grynko et al. fabricated a CdS/P3HT:PCBM/PEDOT:PSS photovoltaic cell to investigate how variations in CdS nanowire morphology affect photovoltaic performance. They reported a highest power conversion efficiency (PCE=0.027%) for two-layer CdS nanowires [9]. Through spray pyrolysis, Yilmaz et al. fabricated CdS thin films on ITO-coated glass substrates, studying the effect of dye modification on CdS surfaces, achieving an overall efficiency of 0.082% for an N719-modified CdS-based solar cell [10]. While many studies examine the structural, optical, and electrical properties of CdS:Co systems, few investigate the device characteristics of CdS:Co thin films in photovoltaic cells. Our research group previously published the only known study on this topic, where we fabricated a photovoltaic cell with Co atoms in the ITO/CdS/N719/P3HT:PCBM/PEDOT:PSS/Ag configuration and found highest PCE=0.488% for CdS:Co thin films [11]. In this paper, however, we put forward a distinct configuration: the ITO/CdS:Co/N719/P3HT/Ag heterostructure.

In this research, CdS and CdS:Co films were grown by chemical bath deposition (CBD) technique on ITO-coated glass substrates. The contribution of Co-doping to the PCE of ITO/CdS/N719/P3HT/Ag solar cells was studied by varying the Co concentration to 0%, 1%, 5%, and 7%. All the resultant data were analyzed and compared to clarify the involvement of Co atoms in enhancing on the performance of CdS-based hybrid photovoltaics.

2. Methods

CdS and CdS:Co films were synthesized by the CBD onto ITO-covered glass slides. The Co-doping concentrations were set at 0%, 1%, 5%, and 7%. ITO substrates, cut to $1 \times 1.25 \text{ cm}^2$, underwent a cleaning process in an ultrasonic bath, followed by sulfuric acid, distilled water, and ethanol treatments for 10 minutes each. Afterward, all slides were blown using a nitrogen gas flow. The CdS growth solution included 0.02 M CdCl_2 , 0.05 M $\text{CH}_4\text{N}_2\text{S}$, 0.05 M NH_4Cl , and NH_4OH dissolved in distilled water, with full preparation details available in our previous paper [11]. The solution was heated up to 75°C on a hot plate and cleaned ITO slides were vertically immersed for 15 minutes to deposit CdS films. For CdS:Co thin films (1%, 5%, and 7% Co), the same procedure was followed, adding 0.02 M $\text{CoCl}_2 \cdot 6\text{H}_2\text{O}$ as a secondary salt. N719 dye was applied to undoped and Co-doped films from a 0.5 mM solution in absolute ethanol using a spin coater at 1000 rpm. P3HT polymer was then coated using a 0.1 g P3HT chlorobenzene solution, also applied at 1000 rpm. Ag paste (area: $0.8 \times 10^{-2} \text{ cm}^2$) was deposited as the front contact, while In metal was used as the back contact. The fabricated devices, designated as Device A (ITO/CdS/N719/P3HT/Ag), Device B (ITO/CdS:Co(1%)/N719/P3HT/Ag), Device C (ITO/CdS:Co(5%)/N719/P3HT/Ag), and Device D (ITO/CdS:Co(7%)/N719/P3HT/Ag), are shown schematically in Fig. 1.

Scanning Electron Microscopy (SEM) (JEOL JSM 6610) instrument was used to examine the morphological characteristics of the devices. Transmittance and absorbance measurements were conducted using a UV-Vis spectrophotometer (SpectraMax M5), which was also used for photoluminescence analysis at an excitation wavelength of 280 nm. The electrical characteristics (J-V) of the fabricated devices were examined with a source meter (Keithley 2410) and a solar simulator (AM 1.5D) operating at a power output of 100 mW/cm^2 .

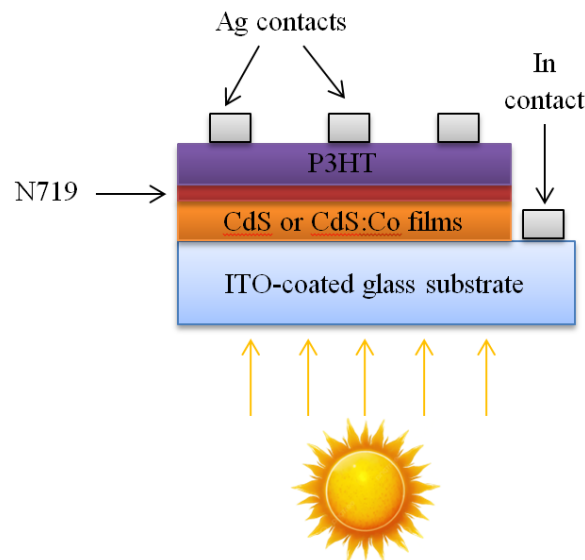


Figure 1. Schematic representation of the fabricated device.

3. Results and Discussion

Figures 2(a)-(d) and (e)-(h) show the surface morphology and cross-sectional images of Devices A, B, C, and D, respectively. In Fig. 2(a), it is observed that the CdS films form spherical structures made up of agglomerated crystallites, with sphere diameters ranging from approximately 0.1 μm to 1 μm , indicating a non-uniform grain size distribution. Notably, each CdS sphere is individually covered by a P3HT layer, rather than being uniformly coated. Device B (Fig. 2(b)) shows a compact, dense, and smooth morphology with reduced grain size, indicating that a low Co-doping concentration (1%) decreases grain size, aligning well with previous reports on CdS:Co films [12]. Some larger grains are also present. Fig. 1(c)-(d) show that Devices C and D have similar surface morphologies, suggesting that increasing the Co concentration up to 7% does not significantly impact grain diameter, shape, or distribution. The microstructure is made up of spherical grains without cracks or pinholes. The individual coverage of P3HT on each CdS sphere remains consistent with Co-doping. Cross-sectional images in Fig. 2(e)-(h) reveal that the thicknesses of Devices A, B, C, and D are approximately 0.52 μm , 0.59 μm , 0.36 μm , and 0.46 μm , respectively.

Figure 3 presents the transmission curves for Devices A, B, C, and D. Device A exhibits low transmittance between 300 and 500 nm, followed by a transmittance range of 5% to 40% from 500 to 650 nm. After 650 nm, Device A's transparency increases, reaching a peak transmittance of 55% at 1000 nm. Conversely, Device B achieves transmittance values above 80% between 650 and 1000 nm, suggesting enhanced transparency likely due to the beneficial effects of Co-doping, consistent with previous reports [13]. Compared to Device A, Device C demonstrates lower transparency, around 70% in the 650-1000 nm range, which may be due to light scattering at grain boundaries because of decreased grain size, which increases boundary lengths [14]. This reduction in transparency might also stem from thickness variations among the devices. Device D shows a transmittance comparable to Device B, exceeding 80%. The absorption edge steepness is often related to the material's crystal quality; thus, Co-doped devices exhibit steeper absorption edges than Device A, indicating Co-doping enhances crystal quality. As indicated by the dashed lines in the figure, an increase in optical transmittance is observed beyond 600 nm for all devices. This behavior confirms that the devices exhibit the characteristic band gap of CdS, which is approximately 2 eV or higher. Additionally, a red shift in the fundamental absorption edge is noted in Devices B, C, and D compared to Device A, suggesting a band gap reduction, likely due to incorporating of Co atoms into CdS host matrix or sp-d exchange interactions between CdS band electrons and the localized d electrons of Co^{2+} ions [15]. An akin band gap diminish was observed in Co-doped CdS nanostructures prepared via spray pyrolysis by Bairy et al. [16]. Overall, Co doping appears to improve the transmittance of devices in the near-infrared (NIR) region.

Figure 4 represents the absorbance data for Devices A, B, C, and D. Device A shows a constant absorbance between 300 nm and 500 nm, followed by a decreasing trend up to 650 nm, corresponding to the band gap of CdS

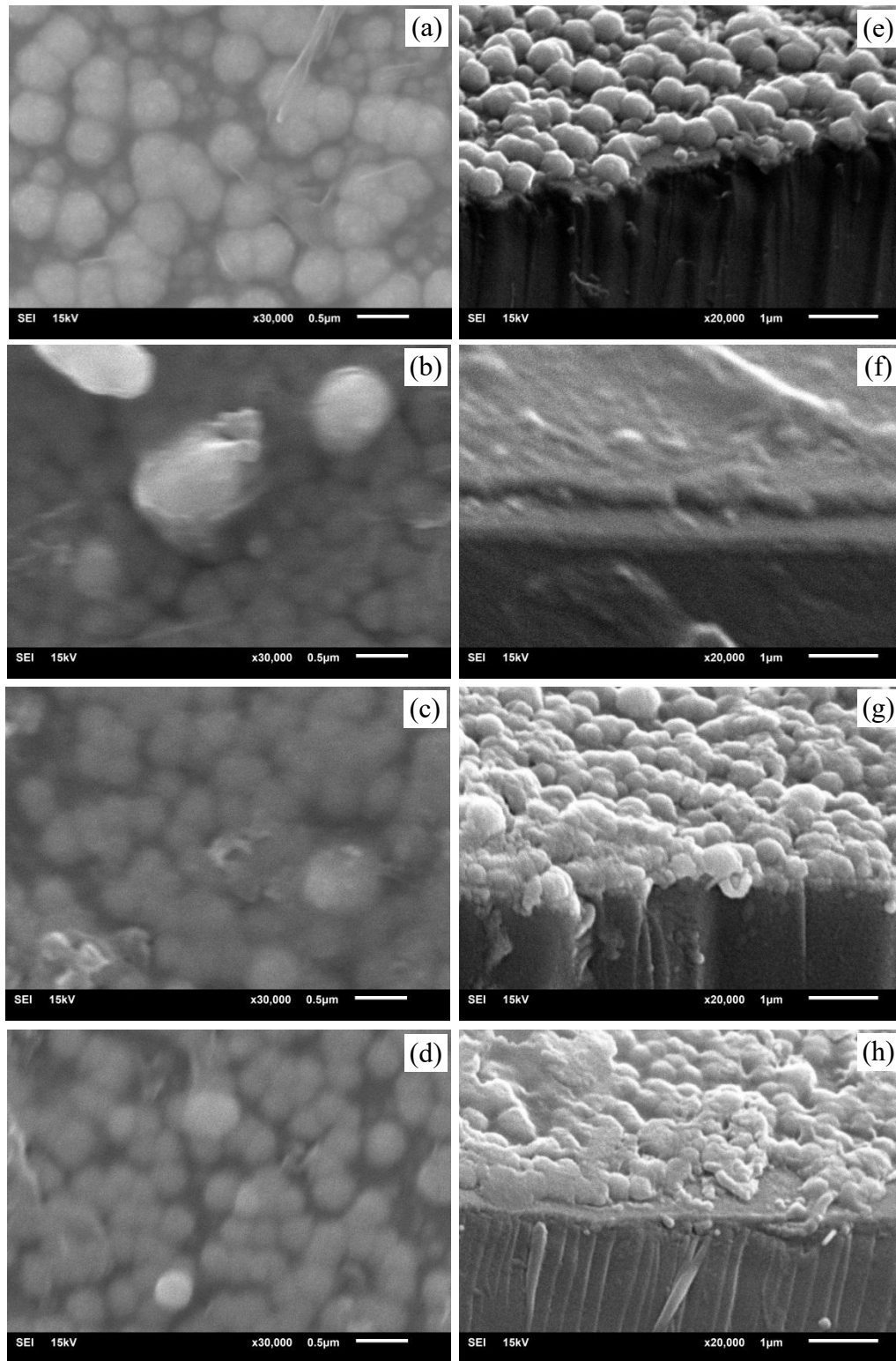


Figure 2. SEM top views of (a) Device A, (b) Device B, (c) Device C, (d) Device D, and cross-sectional views of (e) Device A, (f) Device B, (g) Device C, and (h) Device D.

films. In contrast, Device B exhibits a higher absorption value at 320 nm compared to Device A, but the remainder of the spectrum demonstrates a decreasing trend from 320 nm to 650 nm, remaining lower than that of Device A. Devices C and D display absorption spectra very similar to that of Device B, differing mainly in intensity. Notably, the devices containing Co atoms show lower absorbance than Device A, indicating that the addition of Co atoms to CdS causes a decrement in the absorbance across the spectrum, which aligns with the increased transparency

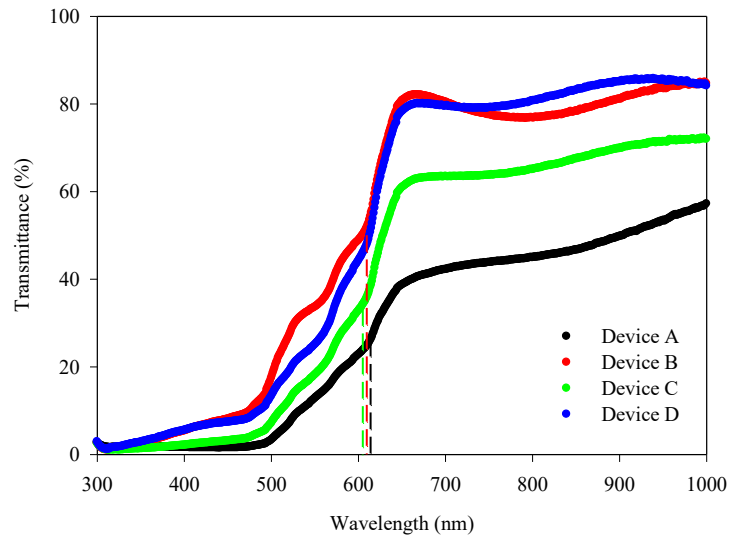


Figure 3. Transmittance data of Device A, Device B, Device C, and Device D.

observed due to Co-doping. This decline in absorption intensity may be attributed to defect states created by the differing sizes of Co^{2+} and Cd^{2+} ions [8]. Deka et al. reported similar findings, noting that the incorporation of Co, Mn, Ni, and Fe atoms decreased the absorbance values of CdS nanocrystals [17]. Conversely, Bairy et al. observed an increment in the absorbance of CdS after Co-doping [16]. Additionally, there appears to be a shift in the fundamental absorption onset of CdS in the devices towards higher wavelengths, which could be associated with a diminish in the band gap, consistent with the findings reported by Maity et al. for CdS:Co quantum dots [18].

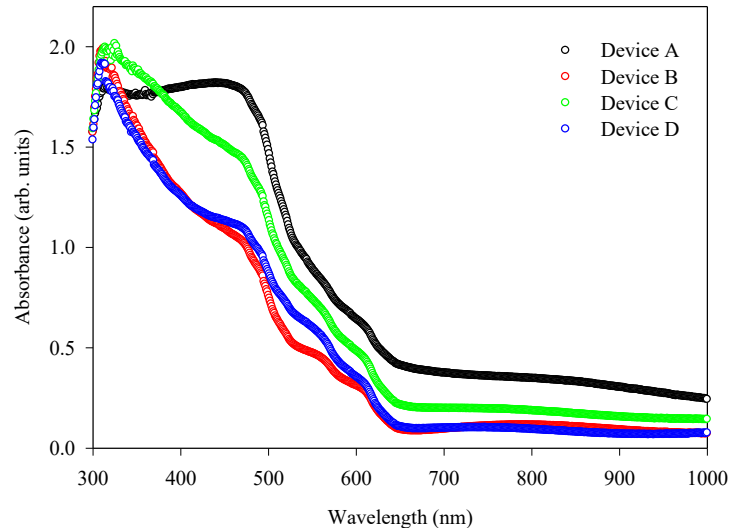


Figure 4. Absorption spectra of Device A, Device B, Device C, and Device D.

Figure 5 demonstrates the photoluminescence (PL) data for Devices A, B, C, D, and the P3HT layer over the range of 300-850 nm. The P3HT layer is observed to dominate the spectra of all the devices in the ranges of 400-500 nm and 600-850 nm, while no peaks corresponding to the 480-600 nm range are detected for the P3HT films. Device A exhibits two distinct peaks at 481 nm and 531 nm. The first peak is referred to radiative transitions occurring between intrinsic defect states and the conduction band, while the second peak could be associated with the band gap of CdS or the Vs defects in the CdS structure [11]. There is no significant change in the peak positions after Co-doping; however, their intensities remarkably decrease, indicating a reduction in the population of these defects. The decrease in PL peak intensity suggests an increase in non-radiative recombination processes, likely due to the formation of additional defect states that act as non-radiative recombination centers. Conversely, the

variation in PL peak intensity in the 600-850 nm range indicates exciton dissociation at the CdS/P3HT interface [19]. Device B shows a more intense peak compared to Device A, implying that poorer exciton dissociation occurs between the CdS and P3HT layers. In contrast, Devices C and D demonstrate less intense peaks than Device A, suggesting that efficient exciton dissociation takes place at the CdS/P3HT interface. Therefore, it can be concluded that a higher amount of Co-doping enhances exciton dissociation in the devices, while a lower amount of Co incorporation has a negative effect.

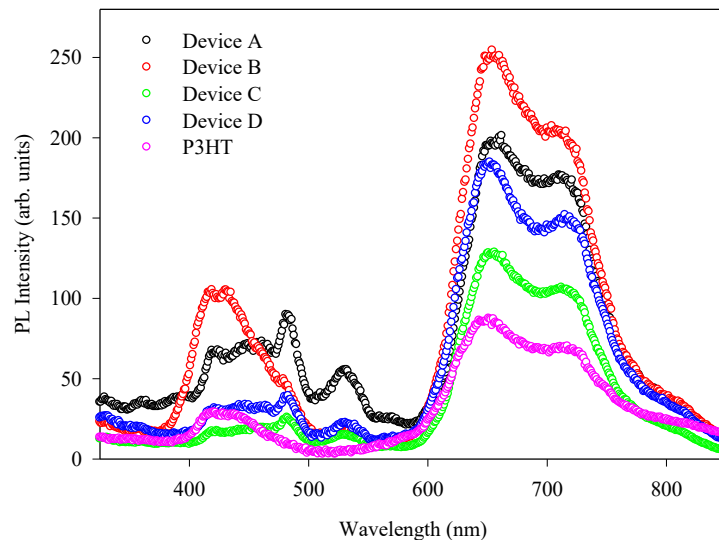


Figure 5. Photoluminescence plots of Device A, Device B, Device C, Device D, and P3HT layer.

Figure 6 presents the J-V characteristics of Device A, Device B, Device C, and Device D, while the solar cell parameters of the devices are summarized in Table 1. Device A shows a short-circuit current density (J_{sc}) of 0.126 mA/cm², an open-circuit voltage (V_{oc}) of 0.115 V, a fill factor (FF) of 0.335, and an overall efficiency of 0.005%. In contrast, the J_{sc} value for Device B significantly decreases to 0.01 mA/cm², although V_{oc} and FF show slight improvements, resulting in an overall PCE of 0.001%. This reduction in efficiency is likely due to poorer exciton dissociation at the CdS:Co/P3HT interface, leading to the formation of fewer e-h pairs, as discussed in the PL analysis. On the other hand, Device C achieves a maximum J_{sc} of 0.197 mA/cm², V_{oc} of 0.371 V, FF of 0.350, and an overall η of 0.028%. This increase in efficiency can be ascribed to the rise in V_{oc} , as listed in Table 1, which suggests effective charge separation between the P3HT and CdS:Co layers, resulting in an increase in e-h pairs. Firoozi et al. reported an increase in J_{sc} for CdS:Co QDs-sensitized solar cells, attributing it to the occurrence of mid-gap states. Device D exhibits slightly lower values than Device C, showing a modest reduction in overall PCE to 0.019%.

Table 1. Photovoltaic parameters of Device A, Device B, Device C, and Device D.

Device's name	J_{sc} (mA.cm ⁻²)	V_{oc} (V)	FF	η (%)
Device A	0.126	0.115	0.335	0.005
Device B	0.014	0.156	0.367	0.001
Device C	0.197	0.371	0.350	0.028
Device D	0.169	0.283	0.355	0.019

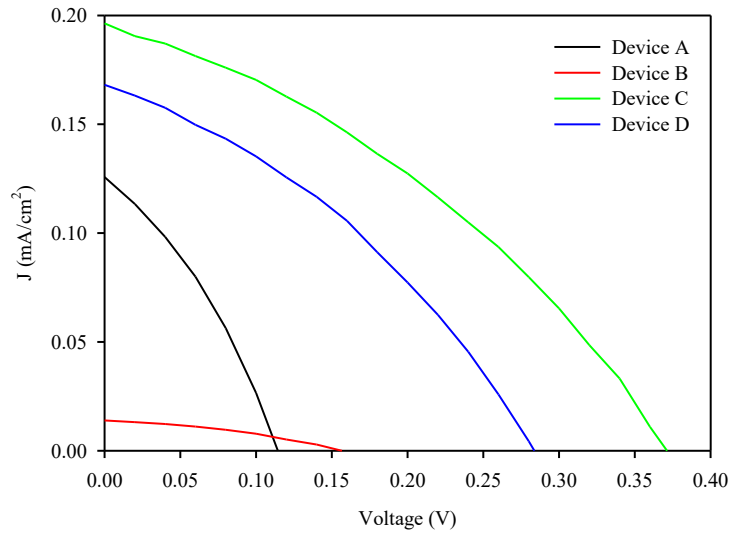


Figure 6. J-V curves of Device A, Device B, Device C, and Device D.

4. Conclusions

This work confirmed the enhancement of PCE in CdS-based hybrid photovoltaics through Co-doping. SEM data indicated that smaller grains were observed for Device B, while Devices C and D exhibited similar surface features to Device A. Devices B and D demonstrated increased transparency in the near-infrared (NIR) region. Photoluminescence (PL) results revealed that Devices C and D had lower PL peaks at higher wavelengths compared to Device A, indicating efficient exciton dissociation occurring between the CdS:Co and P3HT layers. The J-V data showed that a higher concentration of Co-doping caused a significant improvement PCE of the CdS-based photovoltaic cells, with values increasing from 0.005% to 0.028% as the Co concentration rose from 0% to 5%.

Authors' Contributions

SY: Conceptualization, Methodology, Writing - Review & Editing, Validation. **MT:** Data Curation, Writing - Review & Editing. **EB:** Visualization, Investigation, Validation, Writing - Review & Editing, Supervision.

Declaration of Ethical Standards

The author(s) of this article declare that the materials and methods used in this study do not require ethical committee permission and/or legal-special permission.

Conflict of Interest

There is no conflict of interest in this study.




References

- [1] Yılmaz, S., Tomakin, M., Polat, İ., Bacaksız, E., (2023). Facile synthesis and characterization of CdS thin films doped by yttrium atoms, *Applied Physics A* 129, 579.
- [2] Polat, İ., Yılmaz, S., Küçükömeroğlu, T., Tomakin, M., Bacaksız, E., (2024). Performance assessment of oxygenated CdS films-based photodetector. *Materials Today Communications* 38, 107924.
- [3] Vanalakar, S.A., Patil, V.L., Patil, S.M., Deshmukh, S.P., Patil, P.S., Kim, J.H., (2022). Chemical and gas sensing property tuning of cadmium sulfide thin films, *Materials Science and Engineering B* 282, 115787.
- [4] Murai, H., Abe, T., Matsuda, J., Sato, H., Chiba, S., Kashiwaba, Y., (2005). Improvement in the light emission characteristics of CdS:Cu/CdS diodes, *Applied Surface Science* 244, 351–354.

- [5] Rana, M.S., Islam, M.M., Julkarnain, M., (2021). Enhancement in efficiency of CZTS solar cell by using CZTSe BSF layer, *Solar Energy* 226, 272-287.
- [6] Yilmaz, S., Tomakin, M., Ünverdi, A., Aydın, A., Polat, İ., Bacaksız, E., (2020). Structural, morphological, optical analyses of Ni-doped CdS thin films and their photovoltaic performance in hybrid solar cells, *Journal of Materials Science: Materials in Electronics* 31, 12932–12942.
- [7] Han, Y.-X., Yang, C.-L., Sun, Y.-T., Wang, M.-S., Ma, X.-G., (2014). The novel optical properties of CdS caused by concentration of impurity Co, *Journal of Alloys and Compounds* 585, 503-509.
- [8] Pitchaimani, K., Amalraj, L., Muthukumaran, S., (2016). Investigation of structural, photoluminescence and antibacterial behavior of Mn-doped and Co, Mn dual doped CdS thin films by CBD method, *Journal of Materials Science: Materials in Electronics* 27, 12021–12027.
- [9] Grynko, D.O., Fedoryak, O.M., Smertenko, P.S., Ogurtsov, N.A., Pud, A.A., Noskov, Y.V., Dimitriev, O.P., (2013). Application of a CdS nanostructured layer in inverted solar cells, *Journal of Physics D: Applied Physics* 46, 495114.
- [10] Yilmaz, S., Polat, İ., Tomakin, M., Ünverdi, A., Bacaksız, E., (2019). Enhanced efficiency of CdS/P3HT hybrid solar cells via interfacial modification, *Turkish Journal of Physics* 43, 116 – 125.
- [11] Yilmaz, S., Doğan, V., Tomakin, M., Törel, S.B., Polat, İ., Bacaksız, E., (2024). Introduction of Co atoms into CdS thin films for improving photovoltaic properties, *Materials Today Communications* 39, 108805.
- [12] Kumar, S., Sharma, P., Sharma, V., (2014). Redshift in Absorption Edge of $\text{Cd}_{1-x}\text{Co}_x\text{S}$ Nanofilms, *IEEE Transactions on Nanotechnology* 13, 343-348.
- [13] Sharma, B., Lalwani, R., Das, R., (2023). Spectroscopic Studies of CdS Nanocrystalline Thin Films Synthesized by Sol-Gel Spin Coating Technique for Optoelectronic Application: Influence of Co-Doping, *Brazilian Journal of Physics* 53, 42.
- [14] Saravanakumar, S., Chandramohan, R., Premarani, R., Devadasan, J.J., Thirumalai, J., (2017). Studies on Dilute Magnetic Semiconducting Co-Doped CdS Thin Films Prepared by Chemical Bath Deposition method, *Journal of Materials Science: Materials in Electronics* 28, 12092–12099.
- [15] Giribabu, G., Murali, G., Reddy, D.A., Liu, C., Vijayalakshmi, R.P., (2013). Structural, optical and magnetic properties of Co doped CdS nanoparticles, *Journal of Alloys and Compounds* 581, 363-368.
- [16] Bairy, R., Kulkarni, S.D., Murari, M.S., Narasimhamurthy, K.N., (2020). An investigation of third-order nonlinear optical and limiting properties of spray pyrolysis-deposited Co:CdS nanostructures for optoelectronics, *Applied Physics A* 126, 380.
- [17] Deka, K., Kalita, M.P.C., (2018). Structural phase controlled transition metal (Fe, Co, Ni, Mn) doping in CdS nanocrystals and their optical, magnetic and photocatalytic properties, *Journal of Alloys and Compounds* 757, 209-220.
- [18] Maity, P., Singh, S.V., Biring, S., Pal, B.N., Ghosh, A.K., (2019). Selective near-infrared (NIR) photodetectors fabricated with colloidal CdS:Co quantum dots, *Journal of Materials Chemistry C* 7, 7725-7733.
- [19] Zhong, M., Yang, D., Zhang, J., Shi, J., Wang, X., Li, C., (2012). Improving the performance of CdS/P3HT hybrid inverted solar cells by interfacial modification, *Solar Energy Materials and Solar Cells* 96, 160-165.
- [20] Firooz, N., Dehghani, H., Afrooz, M., (2015). Cobalt-doped cadmium sulfide nanoparticles as efficient strategy to enhance performance of quantum dot sensitized solar cells, *Journal of Power Sources* 278, 98-103.



Seasonal analysis of solar energy and hydrogen production potential in Adana

Başak Doğru Mert^{1#} , Hüseyin Nazlıgöl² , Mehmet Erman Mert³ 

Abstract

This study focuses on evaluating the performance of a system comprising an 80W solar panel for electricity generation and hydrogen production via alkaline electrolysis, specifically designed for the Adana region. Simulations conducted in MATLAB/Simulink explored the effects of varying temperature and radiation levels on system performance. The findings reveal a direct correlation between power generation and solar radiation, with higher radiation levels leading to increased power output. However, elevated temperatures negatively impact the efficiency of the PV panel, resulting in reduced power generation. In the experimental setup, graphite (G) and silver-copper-modified graphite (Ag-Cu/G) electrodes were utilized as cathodes, while a platinum electrode served as the anode. Operating voltages ranging from 2.5V to 3V were applied, demonstrating that hydrogen production increases with higher operating voltages. Surface characterization of the electrodes was conducted using SEM-EDX analysis. At 3V, after 15 minutes of operation, hydrogen volumes of 15 mL and 21.4 mL were obtained for G and Ag-Cu/G electrodes, respectively. Seasonal variations were also considered, highlighting that spring's frequent rainy and cloudy conditions limit sunlight availability, whereas the extended clear-sky durations of summer months offer a significant advantage for hydrogen production.

Keywords: Electrocatalyst; Hydrogen; MATLAB/Simulink; PV

¹Adana Alparslan Türkeş Science and Technology University, Department of Energy Systems Engineering, 01250 Adana, Türkiye

ORCID: 0000-0002-2270-9032

²Adana Alparslan Türkeş Science and Technology University, Department of Energy Systems Engineering, 01250 Adana, Türkiye

ORCID: 0000-0003-3037-8568

³Adana Alparslan Türkeş Science and Technology University, Advanced Technology Research and Application Center, 01250 Adana, Türkiye

ORCID: 0000-0002-0114-8707

#Corresponding Author:

E-mail: bdogrumert@atu.edu.tr

Adana ili güneş enerjisi ve hidrojen üretim potansiyelinin mevsimsel analizi

Öz

Bu çalışma, Adana bölgesi için 80W'lık bir güneş paneli kullanılarak elektrik üretimi ve alkali elektroliz yoluyla hidrojen üretimi gerçekleştiren bir sistemin performansını değerlendirmeye odaklanmaktadır. MATLAB/Simulink ortamında gerçekleştirilen simülasyonlar, sıcaklık ve ısıtım seviyelerinin sistem performansı üzerindeki etkilerini incelemiştir. Bulgular, güç üretimi ile güneş ısıtımı arasında doğrudan bir ilişki olduğunu göstermiştir; ısıtım seviyesinin artması, PV panel tarafından üretilen gücü artırmaktadır. Ancak, sıcaklığın artması panel verimliliğini olumsuz etkileyerek üretilen gücün azalmasına yol açmaktadır. Deneysel çalışmada, katot olarak grafit (G) ve gümüş-bakır modifiye grafit (Ag-Cu/G) elektrotlar, anot olarak ise platin elektrot kullanılmıştır. 2,5V ile 3V arasında değişen çalışma voltajları uygulanmış ve hidrojen üretiminin çalışma voltajı arttıkça yükseldiği gözlemlenmiştir. Elektrotların yüzey karakterizasyonu SEM-EDX analizi ile gerçekleştirilmiştir. 3V uygulandığında, 15 dakikalık bir süre sonunda G ve Ag-Cu/G elektrotları için sırasıyla 15 mL ve 21,4 mL hidrojen hacimleri elde edilmiştir. Mevsimsel değişimler de değerlendirilmiştir, ilkbahar mevsimindeki sık yağmurlu ve bulutlu hava koşullarının güneş ışığına erişimi sınırladığı, buna karşın yaz aylarının uzun ve açık hava süreleri sayesinde hidrojen üretimi açısından önemli bir avantaj sunduğu belirlenmiştir.

Anahtar Kelimeler: Elektrokatalizör; Hidrojen; MATLAB/Simulink; PV

Received: 21/01/2025

Revised: 9/02/2025

Accepted: 27/02/2025

Online Published: 20/06/2025

How to Cite: Doğru Mert B., Nazlıgöl H., Mert M.E. "Seasonal Analysis of Solar Energy and Hydrogen Production Potential in Adana" Adana Alparslan Türkeş Science and Technology University Journal of Science, 1 (1): 9-18 (2025).

1. Introduction

Adana, characterized by high solar radiation and extended daylight hours, especially during spring and summer, stands out as one of the most ideal southern provinces in Türkiye for solar energy investments. This region is well-suited for large-scale solar power harvesting due to its advantageous climate and geographic advantages. Adoption of solar energy could be very beneficial for Adana, as it would decrease dependence on fossil fuels by the country, lower current account deficit, and hence lighten the economic burden on households and businesses [1, 2]. Solar energy is a clean, renewable resource that can help prevent global climate change and align well with Türkiye's sustainable development objectives. Enhancing energy security and reducing dependency on external energy sources are two benefits of integrating solar energy into the country's overall energy sources [3, 4]. In this context, solar energy's role in enabling hydrogen production has a critical synergy in the transition toward sustainable energy systems. Hydrogen is a clean and sustainable energy carrier. In contrast to fossil fuels, its utilization in combustion reactions or fuel cells generates only water vapor, leading to zero carbon emissions. This characteristic represents a major advantage in terms of environmental sustainability [5, 6]. Its energy storage capability addresses the intermittent issues of renewable energy sources by balancing supply and demand, thus enhancing the flexibility of energy systems [7, 8]. Furthermore, hydrogen is widely utilized in sectors such as chemistry, industry, and transportation, highlighting its versatility as an energy source [5, 9]. For countries which are reliant on energy imports, producing hydrogen domestically can enhance energy security and support the transition toward energy independence. [10, 11]. Recent cost reductions and technological advancements have made hydrogen economically competitive, accelerating its integration into energy systems and positioning it as a key player in the transition from fossil fuels to clean energy [12]. The produced hydrogen can be currently used for energy storage, transport, and industrial application purposes, therefore making this system altogether versatile in dealing with energy in a sustainable manner [13].

This study highlights the feasibility of utilizing solar energy in Adana and its incorporation into a hybrid energy system for hydrogen production. This system receives converted electricity from solar PV panels to feed an alkali electrolysis unit to produce hydrogen [13, 14]. To evaluate the performance of the solar PV panels under the specific environmental conditions of Adana, simulations were conducted using MATLAB/Simulink. These simulations accounted for critical parameters such as solar radiation levels, ambient temperature, and panel efficiency, which are essential for optimizing hydrogen production [15, 16]. Research has shown that the efficiency of photovoltaic systems can be significantly affected by environmental factors, including temperature and irradiance [17, 18]. As solar irradiance increases, the number of photons absorbed by the solar panels also increases, leading to higher electricity generation. However, high temperatures negatively affect the efficiency of photovoltaic (PV) panels. This phenomenon is primarily due to the increasing energy losses in the semiconductor materials (typically silicon) used in PV panels as temperatures rise. At higher temperatures, the internal resistance of the PV panels increases, which in turn raises the recombination rate of electron-hole pairs. As a result, the open-circuit voltage (Voc) decreases, leading to a reduction in the overall efficiency of the panel. For instance, it has been established that the electrical efficiency of PV panels decreases with increasing temperature, emphasizing the need for effective thermal management strategies [19, 20]. By leveraging the region's favorable solar conditions, Türkiye can enhance its energy independence, reduce greenhouse gas emissions, and contribute to a more sustainable future [21, 22]. The study examines the seasonal usability of solar energy for hydrogen production in the Adana region, with a detailed analysis of the effects of temperature and solar radiation levels on this process. The importance of renewable energy sources in sustainable energy production is growing. In this context, evaluating regional potential and analyzing the hydrogen production process via electrolysis are critical for optimizing energy conversion efficiency. Understanding these factors can contribute to the development of more efficient and sustainable energy systems.

In this study, the integrated small-scale off-grid energy system fitted with an 80W solar photovoltaic panel constitutes the system configuration and provides the electricity supply to the electrolysis unit. The performance of the solar PV panel was simulated using MATLAB/Simulink to check the output for various sunlight and temperature conditions that are typical during both spring and summer months in Adana. Furthermore, different cathode materials were tested to optimize hydrogen production. The actual parameters considered in this study are radiation levels, ambient temperature, electrode efficiency and day duration to calculate the proper hydrogen production.

2. Methods

In this study, an off-grid 80W PV panel system was designed and simulated using MATLAB/Simulink to evaluate its performance in the Adana region during the spring and summer seasons of 2024 (Figure 1). The primary objective was to assess the impact of different climatic conditions on the electricity generated by the PV panel and its subsequent use in hydrogen production through alkaline electrolysis. The technical specifications of the solar PV panel used in the simulations are shown in Table 1.

Table 1. Solar PV panel specifications used in the proposed system

Parameter	Value
Maximum Power (Pmax)	80 W
Open Circuit Voltage (Voc)	21.6 V
Voltage at Maximum Power (Vmp)	17.8 V
Short Circuit Current (Isc)	5.2 A
Current at Maximum Power (Imp)	4.5 A
Number of Cells	36

The simulated solar PV system comprises an 80W monocrystalline solar panel, a charge controller, and a battery storage unit. The generated electricity was supplied to an alkaline electrolysis unit for hydrogen production. In this unit, G and Ag-Cu/G used as cathode electrodes, while platinum was utilized as the anode electrode. Hydrogen production was analyzed for each electrode configuration.

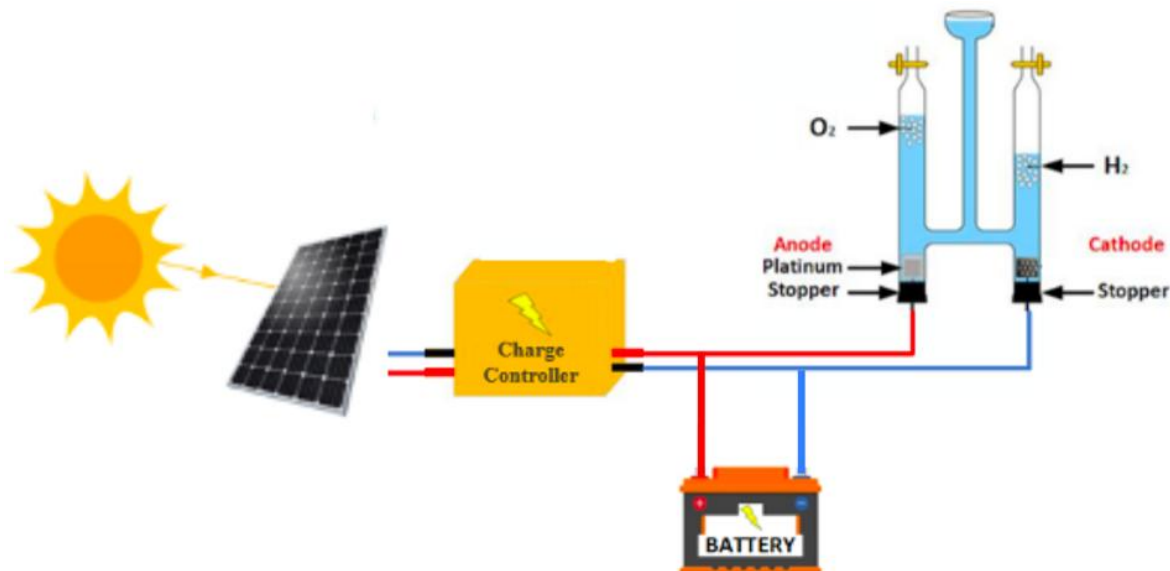


Figure 1. Alkaline electrolysis system powered by solar PV panel.

Climatic data for the Adana region in 2024, including the average number of sunny, cloudy, and rainy days for each month during the spring and summer seasons, were incorporated into the simulations. Data from March, April, and May were used for the spring season, while June, July, and August data were used for the summer season. This information is summarized in Table 2.

Table 2. Number of sunny, cloudy and rainy days in spring and summer

Spring			Summer		
March 2024	5 days		June 2024	1 days	
	Precipitation	Cloudy		Cloudy	Sunny
April 2024	4 days		July 2024	7 days	
	Precipitation	Cloudy		Cloudy	Sunny
May 2024	14 days		August 2024	3 days	
	Precipitation	Cloudy		Cloudy	Sunny

In the simulations, average daily solar radiation levels and temperature variations for each month were considered based on this climatic data. The simulation was conducted based on the data provided in Table 3, which presents the hourly solar radiation and temperature values for sunny, cloudy, and rainy days in the Adana region for 2024. The table classifies each type of day based on the corresponding average temperature and solar irradiance values at different hours. This detailed analysis enables precise modeling of the solar panel's performance under diverse climatic conditions. By incorporating these specific hourly values, the simulation effectively replicated real-world conditions, enabling a comprehensive assessment of how different weather patterns influence the energy generation capacity of the 80W solar panel. This approach ensured that the results reflected the dynamic changes in temperature and radiation levels typical of Adana's seasonal variations, providing a comprehensive understanding of the system's efficiency under different environmental conditions.

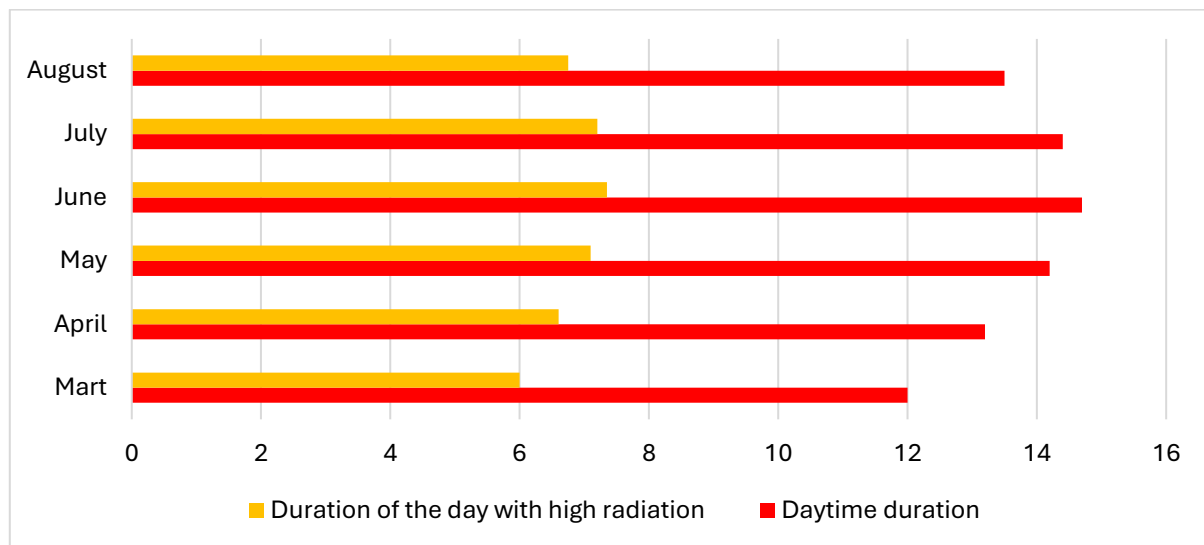
Ag-Cu coating was formed by chronopotentiometry under 50 mA cm⁻² current density [23] in 30% CuSO₄.5H₂O, 1.25% C₄H₆O₆ (tartaric acid), 1.25% AgNO₃, 1.25% H₃BO₃ bath, the counter electrode was Cu sheet %99.9 (1x1x0.2 cm). The operation time was calculated based on Faraday's laws for a film thickness of 10 µm. Electrolysis was conducted using a two-electrode configuration, and the volume of hydrogen gas accumulated at the cathode was measured in an inverted graduated cylinder over a 15-minute period.

3. Results and Discussion

The calculations were carried out considering the daytime durations and the duration of the day with high radiation, as depicted in Figure 2. The red bars represented the total daylight hours for each month from March to August 2024, while the orange bars showed the duration of the day when solar radiation was high enough for efficient energy production. In the simulation, only the hours with high solar radiation were considered for effective energy generation by the 80W solar panel. For instance, in March, although the total daylight duration was around 12 hours, the high radiation period was approximately 6 hours, which was used for power generation calculations. Similarly, for other months, the actual power generation duration was derived from the portion of the day with high radiation, aligning with the brown bars in the graph. This approach ensured that the calculations reflected realistic conditions for solar panel performance, acknowledging that not all daylight hours contribute equally to energy generation. The results thus provided a more accurate representation of the monthly energy production potential of the solar panel under varying radiation conditions throughout the day.

Table 3. Radiation and temperature values in spring and summer

Month	Sunny Days		Cloudy Days		Rainy Days	
	Radiation (W/m ²)	Temp. (°C)	Radiation (W/m ²)	Temp. (°C)	Radiation (W/m ²)	Temp. (°C)
March 2024	840	20	450	18	200	18
April 2024	865	27	460	24	200	24
May 2024	980	32	500	29	200	25
June 2024	1000	36	500	34	200	31
July 2024	1000	40	520	37	200	36
August 2024	980	39	510	37	200	36

**Figure 2.** Daytime duration and effective duration of radiation (hours).

The comparison of monthly energy production revealed significant variations across different months, primarily influenced by the number of sunny, cloudy, and rainy days, as well as the duration of daylight hours with high solar radiation. March, with a total generation of 9567.12 Wh, experienced a relatively balanced distribution of sunny and cloudy days, but its energy production was hindered by rainy days. April saw an improvement with 11204.778 Wh due to an increase in sunny days and longer daylight hours, despite a few additional cloudy days. In contrast, May recorded the lowest total production, 9046.221 Wh, mainly due to a higher frequency of rainy days, which significantly reduced overall energy output, even though daylight hours continued to increase.

Table 4. The total power generation values of sunny, cloudy and rainy days according to the months.

Months	Number of Sunny Days	Power Generation (Wh)	Number of Cloudy Days	Power Generation (Wh)	Number of Rainy Days	Power Generation (Wh)	Total Power Generation (Wh)
March 2024	15	6598.80	11	2496.42	5	471.90	9567.12
April 2024	14	7618.05	12	3186.24	4	400.48	11204.77
May 2024	9	5268.07	8	2281.04	14	1497.09	9046.22
June 2024	24	14303.97	5	1484.7	1	105.10	15913.78
July 2024	21	12254.06	3	872.64	7	720.72	13847.42
August 2024	25	13691.37	3	818.10	3	289.72	14799.20

June marked the peak of energy production at 15913.781 Wh, driven by the highest number of sunny days and the longest daylight duration of 14.7 hours, making it the most productive month for solar energy. July, with 13847.424 Wh, and August, with 14799.2 Wh, also showed high levels of production, benefiting from a similar pattern of extended daylight hours and predominantly sunny days. However, the slight drop in July's total was due to an increase in rainy days compared to June. The results highlight that although the number of sunny days is a key factor, the extended daylight hours and lower cloud coverage during the summer months play a more significant role in enhancing the energy generation potential of solar panels in Adana (Table 4).

In Figure 3, the graph illustrates the power output of an 80W solar panel in Adana, measured in watts, across different weather conditions -sunny, cloudy, and rainy days- from March to August. On sunny days, the panel operated at nearly its maximum capacity, consistently producing around 80W of power. This highlights the optimal performance of the panel under clear-sky conditions. However, on cloudy days, the power output dropped significantly, averaging between 40W to 50W due to reduced solar irradiance. The impact was even more pronounced on rainy days, where the power generation plummets to around 15W-20W, reflecting the minimal sunlight reaching the panel. This data clearly demonstrated how the solar panel's efficiency was directly influenced by weather conditions, with the highest energy production occurring during the summer months of June, July, and August, which had more sunny days. In contrast, the spring months -March, April, and May- experienced lower energy output due to an increased number of cloudy and rainy days. This seasonal variation emphasized the importance of considering local weather patterns when planning for solar energy utilization in Adana.

The FESEM images of the Ag-Cu/G electrode, displayed in Figure 4a–b, highlight its rough surface morphology, which results from the electroplating of Ag and Cu particles. The electrode surface clearly indicates the successful deposition of these metal particles. Additionally, the EDX mapping in Figure 4c demonstrates a uniform distribution of Ag and Cu elements across the surface, confirming the homogeneous nature of the electroplated coating. The Ag and Cu ratio is 4.5 and 95.5%, respectively. The rough and evenly distributed surface is critical for enhancing hydrogen gas production [24-26]. A rough morphology increases the active surface area available for electrochemical reactions, thereby boosting catalytic performance [27-29].

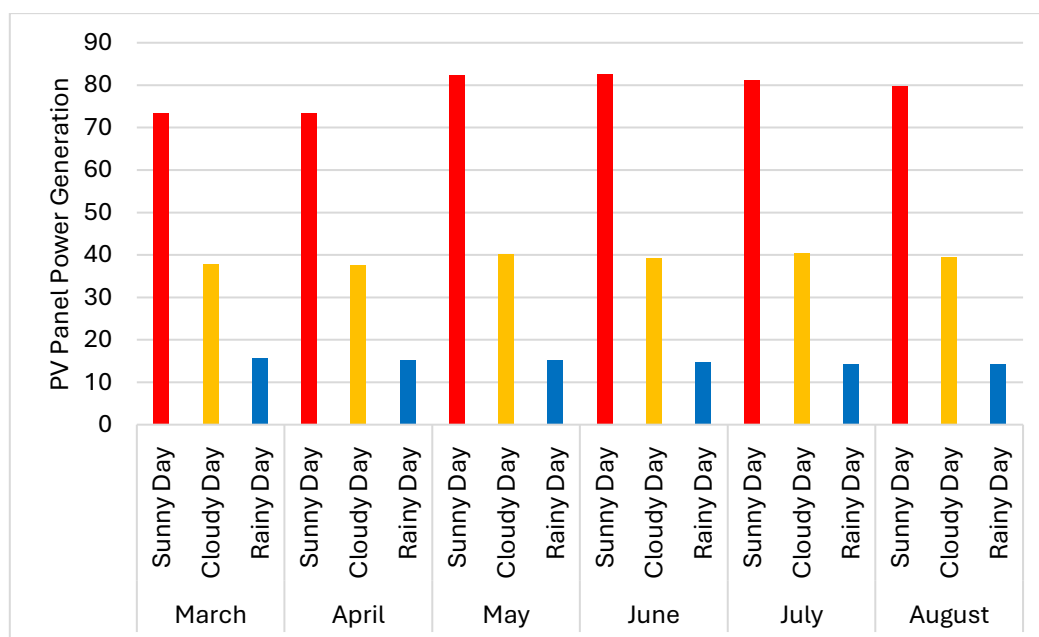


Figure 3. Monthly instantaneous power generation values of 80W solar PV panel according to weather conditions.

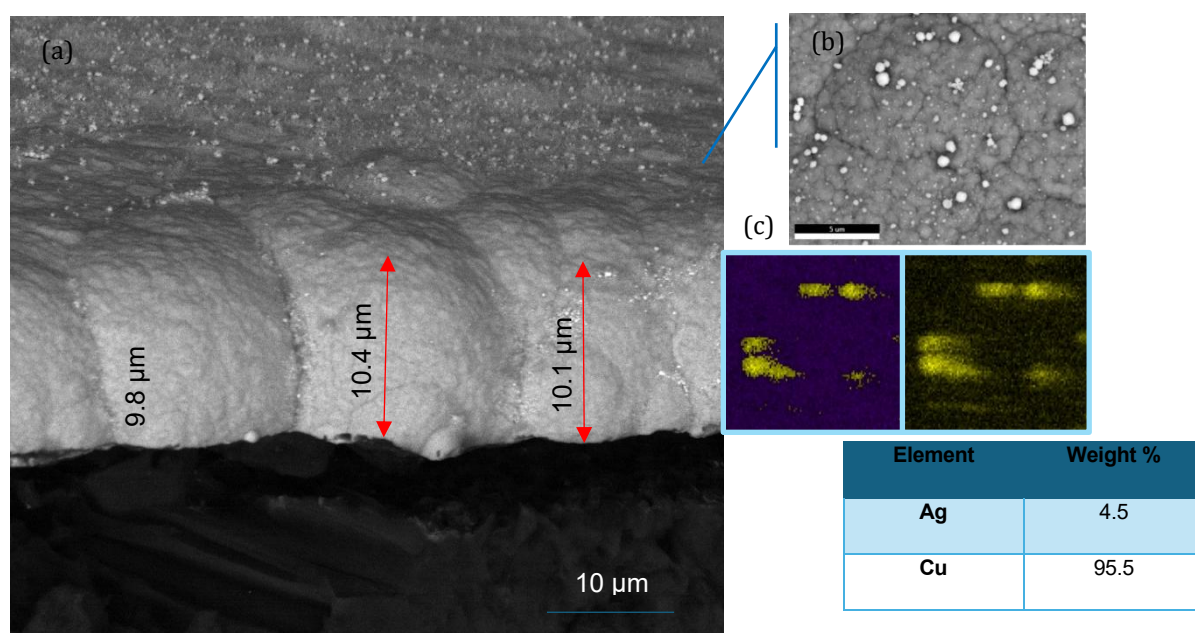


Figure 4. The cross section (a), top view (b) SEM micrograph of catalyst and EDX mapping analysis (c).

Table 5 presented the hydrogen volumes generated during 15 minutes of electrolysis in 1 M KOH at various applied voltages using different cathodes. The G cathode produced 15 mL of hydrogen at 3 V. For the Ag-Cu/G cathode, hydrogen volumes increased progressively with the applied voltage, starting at 13.7 mL cm⁻² at 2.5 V and reaching 21.4 mL cm⁻² at 3 V. This trend demonstrated the enhanced hydrogen production efficiency of the Ag-Cu/G cathode, particularly at higher voltages, compared to the unmodified graphite cathode. The synergistic interaction between Ag and Cu may have contributed to enhanced hydrogen evolution performance. Ag is well-known for its high electrical conductivity and electrocatalytic activity; Cu can help with hydrogen adsorption and desorption procedures, thereby producing a more active catalytic surface. This combination likely improves electron transfer and optimizes the reaction kinetics, leading to the observed increase in hydrogen production.

Table 5. The produced hydrogen volumes.

Cathode@V	V H ₂ / mL cm ⁻²	
G@3.0	15.0	
Ag-Cu/G	@2.5	13.7
	@2.6	15.1
	@2.7	17.3
	@2.8	19.2
	@2.9	20.1
	@3.0	21.4

4. Conclusions

The possibility for producing hydrogen in the Adana region using solar energy was examined in this study, along with the impact of various electrode materials. Alkaline electrolysis and simulations using an 80W solar panel showed that high temperatures have an adverse effect on panel performance and that solar radiation levels directly influence PV panel efficiency. The results showed that energy production was higher in the summer months due to longer daylight hours and a higher number of sunny days. Despite the high temperatures in summer, the increased total solar radiation contributed to higher energy output. In contrast, during the spring months, the high number of rainy and cloudy days limited the total sunlight exposure, resulting in lower energy production. It was observed that the Ag-Cu/G cathode electrode provided the highest hydrogen yield; however, production was lower during the spring months due to limited sunlight hours compared to the summer. These findings highlight the feasibility of hydrogen production using solar energy in regions with high solar potential like Adana, while emphasizing the need to consider seasonal variations and temperature management to enhance system efficiency. In order to enhance the performance of such systems and evaluate their wider applicability, future research should concentrate on a variety of enhancements and integration techniques. These findings are important for optimizing solar energy systems and evaluating the potential for hydrogen production in regions with similar climatic conditions.

Authors' Contributions

BDM: Conceptualization, Methodology, Resources, Writing - Original Draft, Writing - Review & Editing, Validation, Supervision. **HN:** Data Curation, Writing - Original Draft, Software, Validation. **MEM:** Data curation, Visualization, Investigation, Writing - Original Draft.

Declaration of Ethical Standards

The author(s) of this article declare that the materials and methods used in this study do not require ethical committee permission and/or legal-special permission.

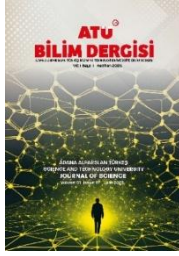
Conflict of Interest

There is no conflict of interest in this study.

References

- [1] Haddad, Z., Nahoui, A., Salmi, M., & Aidjadj, M. (2023). Effect of dust on the operation of photovoltaic solar panels installed in the Hodna region - Experimental study. *Journal of Renewable Energies*, 1, 75–82.
- [2] Koussa, M., Cheknane, A., Hadji, S., Haddadi, M., & Nouredine, S. (2011). Measured and modelled improvement in solar energy yield from flat plate photovoltaic systems utilizing different tracking systems and under a range of environmental conditions. *Applied Energy*, 88, 1756–1771.
- [3] Emetere, M. E., Akinyemi, M. L., & Edeghe, E. B. (2016). A simple technique for sustaining solar energy production in active convective coastal regions. *International Journal of Photoenergy*, 2016, 1–11.
- [4] Tian, Y., & Zhao, C. Y. (2013). A review of solar collectors and thermal energy storage in solar thermal applications. *Applied Energy*, 104, 538–553.
- [5] Mohamed Elshafei, A., & Mansour, R. (2023). Green hydrogen as a potential solution for reducing carbon emissions: A review. *Journal of Energy Research and Reviews*, 13, 1–10.
- [6] Das, A., & Peu, S. D. (2022). A comprehensive review on recent advancements in thermochemical processes for clean hydrogen production to decarbonize the energy sector. *Sustainability*, 14, 11206.
- [7] Lu, L., & Wu, X. (2024). Heteronuclear dual metal atom electrocatalysts for water-splitting reactions. *Molecules*, 29, 1812.
- [8] Li, S., Yang, Z., Shen, Q., & Yang, G. (2023). A parametric study on the interconnector of solid oxide electrolysis cells for co-electrolysis of water and carbon dioxide. *Journal of Marine Science and Engineering*, 11, 1066.
- [9] Yan, F., et al. (2024). Experimental study on the factors influencing performance and emissions of hydrogen internal combustion engines. *E3S Web of Conferences*, 522, 01009.
- [10] Alia, S., Ding, D., McDaniel, A., Toma, F. M., & Dinh, H. N. (2021). Chalkboard 2 - How to make clean hydrogen. *The Electrochemical Society Interface*, 30, 50–56.
- [11] Kanchiralla, F. M., Brynolf, S., Malmgren, E., Hansson, J., & Grahn, M. (2022). Life-cycle assessment and costing of fuels and propulsion systems in future fossil-free shipping. *Environmental Science & Technology*, 56, 12517–12531.
- [12] Li, S., et al. (2022). Techno-economic analysis of sustainable biofuels for marine transportation. *Environmental Science & Technology*, 56, 17206–17214.
- [13] Manoj, V., Pilla, R., & Pudi, V. N. (2023). Sustainability performance evaluation of solar panels using multi-criteria decision-making techniques. *Journal of Physics: Conference Series*, 2570, 012014.
- [14] Sani, M., & Sule, A. (2020). Effect of temperature on the performance of photovoltaic module. *International Journal of Innovative Science and Research Technology*, 5, 670–676.
- [15] Hostin, S., Benedikovic, P., & Michalikova, A. (2009). Chlorine production for water disinfection by means of photovoltaic panels. *Nova Biotechnologica*, 9, 205–210.
- [16] Ma, Y., Li, G., & Tang, R. (2011). Optical performance of vertical axis three azimuth angles tracked solar panels. *Applied Energy*, 88, 1784–1791.
- [17] Chen, X., Wang, W., Luo, D., & Zhu, C. (2019). Performance evaluation and optimization of a building-integrated photovoltaic/thermal solar water heating system for exterior shading: A case study in South China. *Applied Sciences*, 9, 5395.
- [18] Roslan, E., & Hassim, I. (2019). Solar PV system with pulsating heat pipe cooling. *Indonesian Journal of Electrical Engineering and Computer Science*, 14, 311–318.
- [19] Chinathambi, G., Murugesan, M., Palanisamy, C., Munirajan, S., & Bhero, S. (2017). Modeling of a solar photovoltaic water pumping system under the influence of panel cooling. *Thermal Science*, 21, 399–410.
- [20] Mejia, F. A., & Kleissl, J. (2013). Soiling losses for solar photovoltaic systems in California. *Solar Energy*, 95, 357–363.
- [21] Matuska, T., & Sourek, B. (2017). Performance analysis of photovoltaic water heating system. *International Journal of Photoenergy*, 2017, 1–10.
- [22] Song, J., Zhu, Y., Xia, D., & Yang, Y. (2014). A photovoltaic solar tracking system with bidirectional sliding axle for building integration. *Energy Procedia*, 61, 1638–1641.
- [23] Mert, M. E., & Kardaş, G. (2011). Electrocatalytic behaviour of NiBi coatings for hydrogen evolution reaction in alkaline medium. *Journal of Alloys and Compounds*, 509, 9190–9194.
- [24] Zhao, H., Liu, M., Du, X., & Zhang, X. (2024). Synthesis of M-NiS/Mo₂S₃ (M = Co, Fe, Ce, and Bi) nanoarrays as efficient electrocatalytic hydrogen evolution reaction catalyst in fresh and seawater. *International Journal of Hydrogen Energy*, 62, 532–540.
- [25] Zhang, J., Cui, W., Ni, Y., Chen, W., & You, D. (2024). A MoS₂/Cu_{1.8}S/NiS@MoSX heterostructured electrocatalyst for high-efficiency hydrogen evolution in alkaline solution. *International Journal of Hydrogen Energy*, 51, 1577–1585.
- [26] Wang, C., et al. (2024). Advanced noble-metal/transition-metal/metal-free electrocatalysts for hydrogen evolution reaction in water-electrolysis for hydrogen production. *Coordination Chemistry Reviews*, 514, 215899.

- [27] Kumar Mandari, K., & Kang, M. (2024). CuNi-LDH sheets and CoS nanoflakes decorated on graphitic carbon nitride heterostructure catalyst for efficient photocatalytic H₂ production. *Applied Surface Science*, 655, 159550.
- [28] Guo, L., et al. (2024). Self-supported crystalline-amorphous composites of metal phosphate and NiS for high-performance water electrolysis under industrial conditions. *Applied Catalysis B: Environmental*, 340, 123252.
- [29] Zhang, K., Yang, E., Zheng, Y., Yu, D., Chen, J., & Lou, Y. (2023). Robust and hydrophilic Mo-NiS@NiTe core-shell heterostructure nanorod arrays for efficient hydrogen evolution reaction in alkaline freshwater and seawater. *Applied Surface Science*, 637, 157977.



Green synthesis of ZnO nanoparticles using pine bark extract

Faruk Aslan^{1#} , Ahmet Ekicibil² 

Abstract

In this study, zinc oxide (ZnO) nanoparticles (NPs) were synthesized by green synthesis technique using pine bark extract. ZnO NPs were synthesized in three different pine bark extract ratios, which acts as a reducing and stabilizing agent. The produced ZnO NPs were characterized using X-ray diffraction (XRD), scanning electron microscopy (SEM), energy dispersive X-ray spectrum analysis (EDS) and ultraviolet-visible light spectroscopy (UV-VIS). It was determined that the XRD diffraction peaks were consistent with the characteristic peaks of ZnO, and ZnO NPs were produced in the hexagonal wurtzite crystal phase. It was determined from the SEM images that the samples were produced homogeneously which have almost spherical geometry and the average particles were in the range of 20-30 nm. In the elemental analysis, only Zn and O elements were observed without any impurity atoms. Also, the degradation performance of methylene blue (MB) dye under UV light was determined to determine the photocatalytic activities of ZnO NPs. It was determined that MB reached almost 66% degradation efficiency after 80 minutes of UV illumination of ZnO NPs synthesized by using pine bark extract.

Keywords: ZnO; Green synthesis; Pine bark; Optical properties; Photocatalytic activity

¹Çukurova University, Department of Physics, 01330 Adana, Türkiye

ORCID: 0009-0007-5012-8941

¹Çukurova University, Department of Physics, 01330 Adana, Türkiye

ORCID: 0000-0003-3071-0444

#Corresponding Author:

E-mail: farukaslan22@gmail.com

Received: 18/02/2025

Revised: 20/03/2025

Accepted: 4/11/2025

Online Published: 20/06/2025

How to Cite: Aslan F., Ekicibil A., "Green Synthesis of ZnO Nanoparticles Using Pine Bark Extract" Adana Alparslan Turkey Science and Technology University Journal of Science, **1** (1): 19-27 (2025).

Çam kabuğu ekstraktı kullanılarak ZnO nanopartiküllerinin yeşil sentezi

Öz

Bu çalışmada, çinko oksit (ZnO) nanoparçacıkları (NPs) çam kabuğu özütü kullanılarak yeşil sentez tekniği ile üretilmiştir. İndirgeyici ve dengeleyici bir madde olarak görev alan çam kabuğu özütü üç farklı oranda kullanılarak ZnO NP'leri sentezlenmiştir. Üretilen ZnO NP'leri X-ışını kırınımı (XRD), taramalı elektron mikroskobu (SEM), enerji dağılımlı X-ışını spektrum analizi (EDS) ve ultraviyole-görünür ışık spektroskopisi (UV-VIS) kullanılarak karakterize edildi. XRD kırınım piklerinin ZnO'nun karakteristik pikleriyle uyumlu olduğu ve hegzagonal wurtzit kristal fazında üretildiği belirlendi. SEM görüntülerinden numunelerin homojen bir şekilde üretildiği, parçacıkların hemen hemen küresel geometriye sahip olduğu ve ortalama parçacık boyutunun 20-30 nm aralığında olduğu belirlendi. Elementel analizde sadece Zn ve O elementleri gözlenerek, safsızlık atomlarının bulunmadığı tespit edildi. Ayrıca, ZnO NP'lerinin fotokatalitik aktivitesinin belirlenmesi için UV ışığı altında metilen mavisi (MB) boyasının bozunma performansı incelendi. Çam kabuğu özütü kullanarak sentezlenen ZnO NP'lerinin 80 dakikalık UV aydınlatması sonrasında MB'yi yaklaşık %66 oranında bozunma aktivitesine ulaştırdığı belirlendi.

Anahtar Kelimeler: ZnO; Yeşil sentez; Çam kabuğu özütü; Optik özellikler; Fotokatalitik aktivite

1. Introduction

Nanotechnology, a field of intense interest today, traces its roots back to Michael Faraday's paper published in 1857 [1]. Nanotechnology has a wide range of applications, with primary uses in environmental and industrial sectors [2]. The sustainable use of natural resources is one of the most urgent environmental issues of our time. Increasing population and industrial activities are escalating environmental pressures, deepening pollution problems that threaten our water resources. Industrial waste, particularly harmful dyes such as the commonly used methylene blue, are among the primary pollutants. These dyes pose significant risks to both human health and ecosystems. Protecting water resources and effectively removing pollutants are vital for the continuation of healthy ecosystems [3].

All methods, except for green synthesis, have disadvantages such as high costs and the formation of toxic by-products. In contrast, the green synthesis method offers an environmentally friendly, non-toxic, and more cost-effective alternative, making it more advantageous compared to other chemical and physical methods [4].

ZnO nanoparticles are widely utilized in various fields such as electrochemistry, medical devices, and the textile industry due to their high specific surface area, ultraviolet light absorption, and scattering properties. The synthesis of ZnO nanoparticles is typically categorized into physical and chemical methods, which often involve high energy consumption, low purity, irregular particle size distribution, high production costs, substantial secondary waste generation, and irreversible environmental pollution. As the applications of ZnO nanoparticles continue to expand, their synthesis through environmentally friendly methods has become a significant concern, primarily due to the increasing importance of environmental protection in societal expectations. Green synthesis methods are eco-friendly alternatives that utilize natural resources, such as plant extracts, during the production process. Plant extracts provide a sustainable and eco-friendly substitute for conventional chemical approaches in green synthesis processes. Because of its abundance of bioactive components, pine bark extract is a noteworthy natural reducing and stabilizing agent in this context. Pine bark, which is rich in phenolic compounds, supports the reduction of metal ions through its strong antioxidant activity, which aids in the creation of nanoparticles. Pine bark's organic components, which include functional groups like hydroxyl and carbonyl, allow it to bind metal ions and serve as a stabilizing and reducing agent in green synthesis. Taking all these elements into account, the application of pine bark extract in green synthesis is thought to be a creative and sustainable method from an economic, scientific, and environmental standpoint [5].

Plants and their extracts are readily accessible resources, and the process requires only the use of a zinc salt solution as the metal precursor. ZnO nanoparticles are synthesized through the reaction of plant extracts with a zinc salt solution. This method offers a highly suitable approach for the green synthesis of ZnO nanoparticles. In addition, studies in the literature were reviewed. Karnan et al. synthesized ZnO nanoparticles using *Nephelium lappaceum* L. plant extract and achieved 83.99% successful reduction to methylene blue dye [6]. Soto-Robles et al. synthesized ZnO nanoparticles using *Corymbia Hibiscus sabdariffa* extract and achieved 98.6% successful reduction to methylene blue dye [7]. Zheng et al. synthesized ZnO nanoparticles using *Corymbia citriodora* plant extract and achieved 83.45% successful reduction to methylene blue dye [8].

In this study, we report the synthesis of ZnO nanoparticles using pine bark extract and zinc salt as precursors as an original and unprecedented study among numerous studies. The structural properties of the synthesized ZnO nanoparticles were verified using UV-Vis, XRD (X-Ray Diffraction), SEM (Scanning Electron Microscopy) and EDX (Energy Dispersive X-ray Analysis) techniques [7].

2. Methods

2.1 Materials

Pine bark extract was utilized instead of reducing and stabilizing agent chemicals for the green synthesis of the ZnO samples. Distilled water was employed for the synthesis. The zinc nitrate hexahydrate ($\text{Zn}(\text{NO}_3)_2 \cdot 6\text{H}_2\text{O}$, Sigma-Aldrich, 99%) was used as Zn source.

2.2 Synthesis of particles

ZnO particles were produced by the green synthesis method as shown in Figure 1. 1.0 gr of zinc nitrate hexahydrate salt was completely dissolved in 15 ml of distilled water within a 50 ml beaker using an ultrasonic

bath. 1.0 gr of pine bark extract was also dissolved in 13 ml of distilled water within a 50 ml beaker using an ultrasonic bath. Subsequently, the well-mixed solutions were combined by placing the beaker containing the zinc nitrate salt on a magnetic stirrer and adding the pine bark extract drop by drop. The mixture was stirred at 150 °C until the solution reached a gel-like consistency. The gel was then subjected to calcination by placing it in an oven at 500 °C for 2 hours. After the calcination process, the samples were ground with an agat mortar for a total of 20 minutes and then placed into tubes for measurements. The sample produced as explained above is labelled as ZnO-PB2. The same process was repeated two more times to change the concentration of pine bark extract. Changing the concentration in the samples is intended to have a direct impact on the physicochemical characteristics of the nanoparticles in the green synthesis process, which may result in notable modifications. The reduction rate of metal ions increases with extract concentration, perhaps resulting in the production of smaller nanoparticles. On the other hand, the growth process moves more slowly at lower concentrations, producing larger and more asymmetrical structures. Samples were made at varying concentrations as a result. Other samples were prepared by dissolving the pine bark extract in 7.0 ml of distilled water (ZnO-PB1) and 19 ml of distilled water (ZnO-PB3).

Production steps ZnO nanoparticles

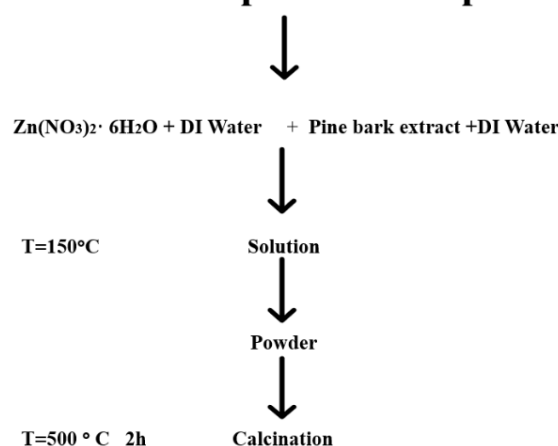


Figure 1. Production scheme of ZnO nanoparticles.

2.3 Characterization techniques

The structural properties of ZnO NPs synthesized via green synthesis were investigated using a Rigaku MiniFlex 600 model XRD system with Cu-K α radiation (wavelength $\lambda = 1.5406 \text{ \AA}$). Subsequently, the morphology, surface properties and elemental analysis of the ZnO nanoparticles were examined using a SEM and EDS with an FEI-QUANTA650. The UV-VIS spectrophotometer, which measures in the wavelength range of 300-800 nm, was used to examine the optical characteristics of ZnO nanoparticles.

3. Results and Discussion

The X-ray diffraction technique was used to identify and describe the crystalline phase of the ZnO nanoparticles (Fig.2). The diffraction patterns of the ZnO-PB1, ZnO-PB2, and ZnO-PB3 samples exhibit sharp and well-defined peaks, indicating their highly crystalline structure. Although the concentration of pine bark extract was different in ZnO-PB1, ZnO-PB2, and ZnO-PB3 samples, the diffraction peaks of them are almost same. This means that the working concentration of pine bark extract were not affected the crystal formation of ZnO NPs. However, the peak intensities changes by the concentration of pine bark extract. The maximum peak intensity was seen in ZnO-PB2 sample. Different diffraction peaks at the 2θ values of 32.11° , 34.76° , 36.59° , 47.85° , 56.91° , 63.16° , 66.68° , 68.24° , 69.38° , 72.54° , and 76.92° are visible in the X-ray diffraction patterns of the green synthesis nanoparticles. These peaks are indexed to the (100), (002), (101), (102), (110), (103), (200), (112), (201), (004), and (202) planes, respectively. The hexagonal wurtzite crystal structure that characterizes ZnO nanoparticles is represented by these peaks [9].

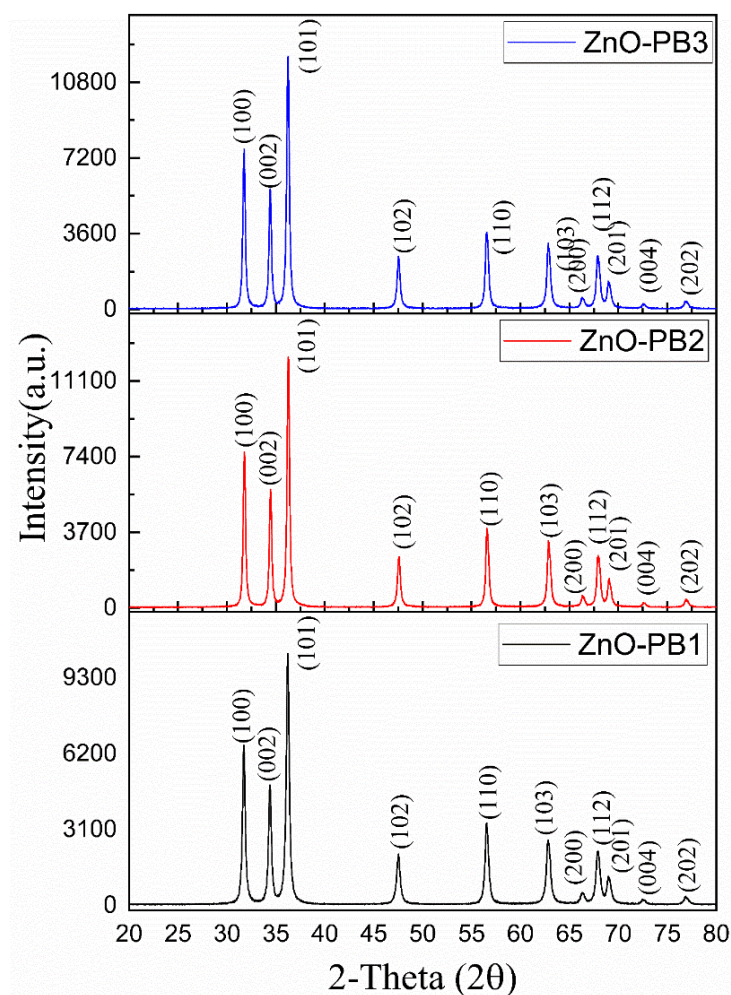


Figure 2. XRD patterns of the ZnO samples.

The Debye-Scherrer formula can be used to determine the crystal size:

$$D = \frac{\kappa\lambda}{\beta \cos\theta} \quad (1)$$

where θ is the Bragg angle, β is the full width at half-maximum peak intensity (FWHM), λ is the x-ray wavelength, D is the average crystallite size, and κ is a dimensionless value that is about equal to 0.9 [10]. The average crystallite sizes of samples calculated from the XRD data were found as 24, 39, and 27 nm for ZnO-PB1, ZnO-PB2, and ZnO-PB3, respectively. These results show that the amount of extract used affects the crystal size of ZnO NPs.

2.1 Surface morphology and elemental analysis

Since the crystal property of samples are similar, the ZnO-PB2 sample was selected for surface morphology and elemental analysis measurements. SEM images taken at various magnifications for ZnO-PB2 sample are shown in Fig.3(a-d). SEM images were taken at 50kx, 100kx, 200kx, 400kx magnifications under 20kV. It was observed that the surface morphology of the ZnO nanoparticles was close to spherical grains and exhibited a homogeneous distribution. The morphology of our green-synthesized sample is consistent with the literature [11]. In addition, the grain size distribution of ZnO-PB2 sample was drawn by randomly selected 100 grains in the SEM images.. Figure 3(e) shows the grain size distribution of ZnO-PB2 sample. The average grain size of the ZnO-PB2 sample was found in the range of 20-30 nm.

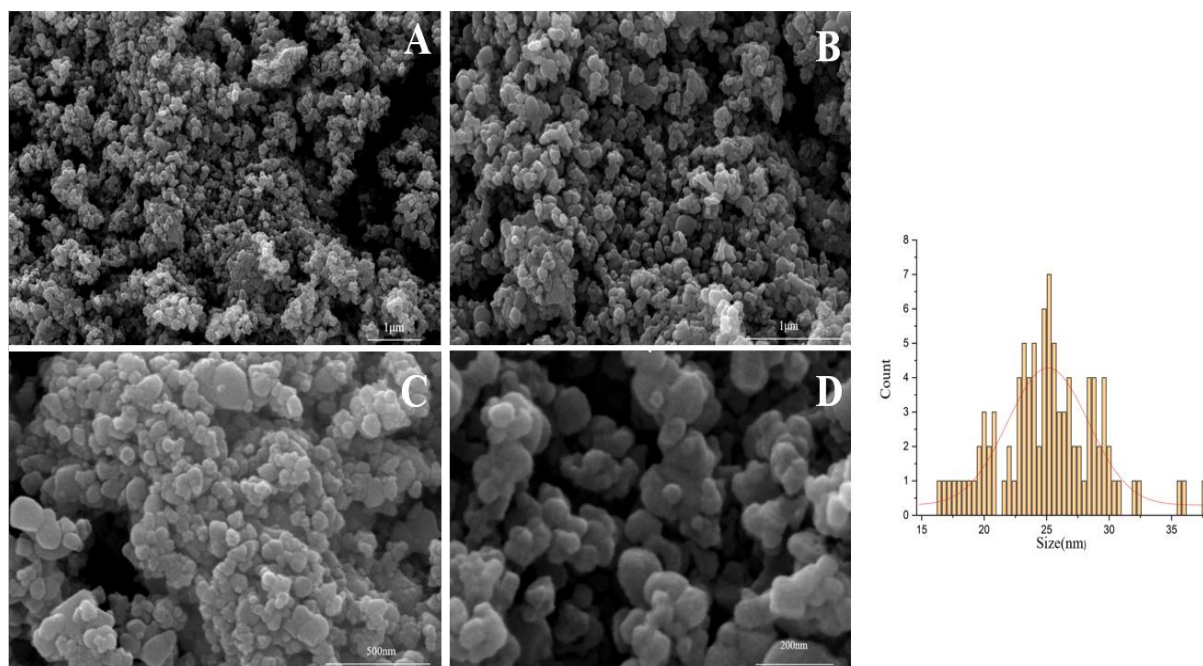


Figure 3. SEM images and nanoparticle size analysis of the sample coded ZnO-PB2.

To determine the elemental composition of the ZnO nanoparticles, EDS analysis was performed. Figure 4 shows the EDS spectrum and elemental analysis results of the ZnO-PB2 sample. In the spectrum, Zn, O, Ca and C elements were detected. The C peak might come from the carbon sample holder. The reason of observing Ca peaks might be related to the insufficient washing procedure. Zn and O elements are almost equal atomic % that it confirms the formation of ZnO structure.

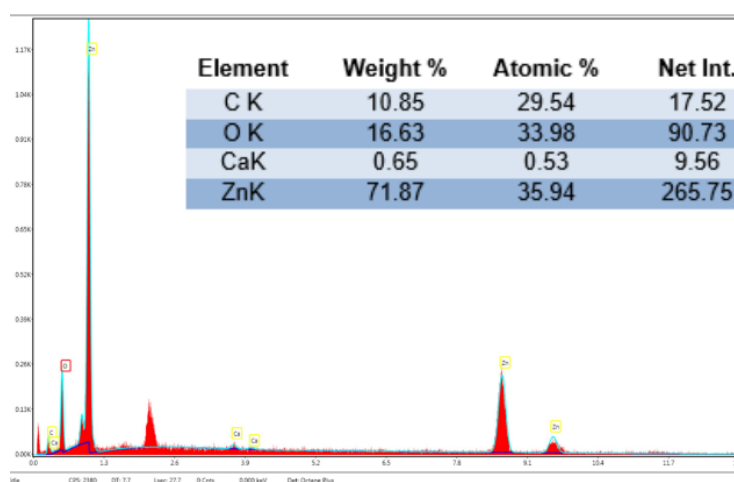


Figure 4. EDS images sample coded ZnO-PB2.

2.2 Photocatalytic activity

The photocatalytic activity of ZnO nanoparticles synthesized using green methods with pine bark extract was examined the degradation of methylene blue under ultraviolet light irradiation. All experiments were performed at room temperature and the spectrum was taken every 10 minutes up to total 80 minutes. The UV-VIS adsorption variations in the presence of ZnO-PB1, ZnO-PB2, and ZnO-PB3 photocatalysts are depicted in Figure 5(a-c), respectively. In the spectra, an absorbance peak originating from the MB solution was observed at 664 nm. The majority of the methylene blue solutions' discoloration happens in the presence of the photocatalyst within 80 minutes, based on variations in absorbance intensity during the course of the reaction. Figure 5(d) displays the

percentages of photocatalytic methylene blue dye degradation for each of the ZnO-PB1, ZnO-PB2, and ZnO-PB3 samples in a reactor over an 80-minute period. The degradation process was split into two stages. The first stage involved keeping the dye/catalyst solution at a steady temperature for 20 minutes without using the UV lamp. During an 80-minute reaction time in the second stage (with the UV lamp turned on), the ZnO-PB3 sample is found to have the maximum photocatalytic activity (33%), in contrast to the ZnO-PB1 and ZnO-PB2 samples (6% and 7%, respectively).

In contrast to ZnO nanoparticles made with other green reducing agents, these results validate the partially effective synthesis of ZnO nanoparticles employing pine bark extract. A comparison with other ZnO research conducted for the degradation of organic contaminants is presented in Table 2.

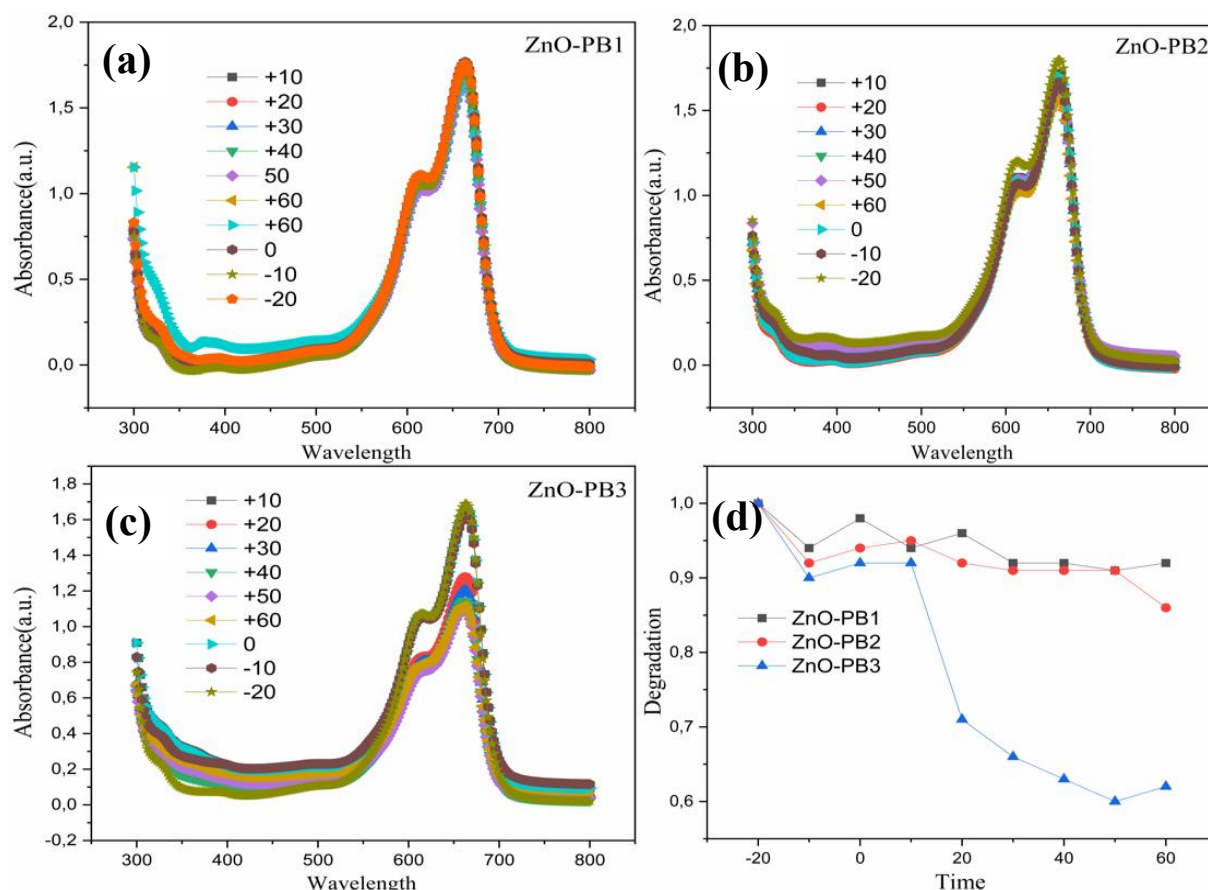


Figure 5(a-c). The absorbance spectra of methylene blue as a function of wavelength of radiation for ZnO-PB1, ZnO-PB2 and ZnO-PB3, respectively. (d) The degradation percentage of methylene blue as a function of time for ZnO-PB1, ZnO-PB2 and ZnO-PB3 samples.

4. Conclusions

This work explores the green synthesis of ZnO nanoparticles using pine bark extract. The amount of extract used during synthesis influenced the crystallite size of ZnO nanoparticles. The morphology of the samples has formed in a spherical shape. Additionally, the characteristic diffraction peaks were successfully obtained in the XRD results, and it confirms our green synthesis ZnO nanoparticles fit with the other synthesis processes. Furthermore, the ZnO materials demonstrated good photocatalytic activity, achieving 34% degradation of methylene blue within 80 minutes. It is promising that the ZnO nanoparticles obtained by green-synthesizing process using pine bark extract for the first time show photocatalytic activity at a level comparable to the literature.

Table 2. Comparative chart of ZnO nanoparticles synthesized using different plants.

Number	Biological entity	Pollutant	Degradation Efficiency	Time of Degradation	Reference
1	Pithecellobium dulce peel	MB	63%	120 min	[12]
2	Pyrus pyrifolia	MB	80.30%	210 min	[13]
3	Suaeda japonica Makino	MB	54%	60 min	[14]
4	Camellia sinensis powder	MO	80%	180 min	[15]
5	Coriandrum sativum	-	81.90%	240 min	[16]
6	Phoenix dactylifera waste	EY	90.6%	180 min	[17]
7	Salvadora persica leaf	MB	95%	150 min	[18]
8	Syzygium cumini leaf	MB	91.4%	180 min	[19]
9	Tabernaemontana divaricate leaf	MB	100%	90 min	[20]
10	Buchanania lanzan leaf	MG	95%	150 min	[21]
11	Garcinia cambogia fruit	MB	81.5%	90 min	[22]
12	Hibiscus sabdariffa	MB	97%	150 min	[23]
13	Scutellaria baicalensis	MB	98.6%	210 min	[24]
14	Corymbia citriodora	MB	83.45%	90 min	[8]

Acknowledgement

This work was supported by the Scientific and Technological Research Council of Türkiye (TÜBİTAK) under project number 2209-A, number 1919B012300077.

Authors' Contributions

FA: Conceptualization, Methodology, Writing - Original Draft, Software. **AE:** Writing - Review & Editing, Validation, Supervision.

Declaration of Ethical Standards

The author(s) of this article declare that the materials and methods used in this study do not require ethical committee permission and/or legal-special permission.

Conflict of Interest

There is no conflict of interest in this study.




References

- [1] Thompson, D.J.G.B., (2007). Michael Faraday's recognition of ruby gold: the birth of modern nanotechnology: His 1857 lecture to the royal society in London. 40(4), 267-269.
- [2] Durmuş, S., Keleşoğlu, G.S., Özdiñer, M., Dalmaz, A., and Zenkin, K., (2023). Green synthesis and structural characterization of ZnO nanoparticle and ZnO@TiO₂ nanocomposite by Cinnamomum verum bark extract. Turkish Journal of Analytical Chemistry, 5(2), 118-123.
- [3] İşlek, D., (2023). Çinko oksit nanopartiküllerinin yeşil sentezi, karakterizasyonu, sitotoksitesi ve antimikrobiyal aktivitesi Afyon Kocatepe University. p. 97.
- [4] Sağlam, Ö., (2024). İncir yaprağı ekstreğinden yeşil sentez yöntemi ile zno ve Fe, MN katkılı ZnO nanoparçacıklarının fotovoltaiik ve fotokatalitik uygulamaları ve karakterizasyonu Siirt Üniversitesi. p. 57.
- [5] Xu, J., Huang, Y., Zhu, S., Abbes, N., Jing, X., Zhang, L.J.J.o.E.F., and Fabrics, (2021). A review of the green synthesis of ZnO nanoparticles using plant extracts and their prospects for application in antibacterial textiles. 16, 15589250211046242.
- [6] Karnan, T. and Selvakumar, S.A.S.J.J.o.m.S., (2016). Biosynthesis of ZnO nanoparticles using rambutan (Nephelium lappaceumL.) peel extract and their photocatalytic activity on methyl orange dye. 1125, 358-365.
- [7] Fakhari, S., Jamzad, M., Kabiri Fard, H.J.G.c.l., and reviews, (2019). Green synthesis of zinc oxide nanoparticles: a comparison. 12(1), 19-24.
- [8] Zheng, Y., Fu, L., Han, F., Wang, A., Cai, W., Yu, J., Yang, J., Peng, F.J.G.C.L., and Reviews, (2015). Green biosynthesis and characterization of zinc oxide nanoparticles using Corymbia citriodora leaf extract and their photocatalytic activity. 8(2), 59-63.
- [9] Davar, F., Majedi, A., and Mirzaei, A.J.J.o.t.A.C.S., (2015). Green synthesis of ZnO nanoparticles and its application in the degradation of some dyes. 98(6), 1739-1746.
- [10] Suresh, D., Shobharani, R., Nethravathi, P., Kumar, M.P., Nagabhushana, H., Sharma, S.J.S.A.P.A.M., and Spectroscopy, B., (2015). Artocarpus gomezianus aided green synthesis of ZnO nanoparticles: Luminescence, photocatalytic and antioxidant properties. 141, 128-134.
- [11] Steffy, K., Shanthi, G., Maroky, A.S., and Selvakumar, S.J.J.o.a.r., (2018). Synthesis and characterization of ZnO phytonanocomposite using Strychnos nux-vomica L.(Loganiaceae) and antimicrobial activity against multidrug-resistant bacterial strains from diabetic foot ulcer. 9, 69-77.
- [12] Madhumitha, G., Fowsiya, J., Gupta, N., Kumar, A., Singh, M.J.J.o.P., and Solids, C.o., (2019). Green synthesis, characterization and antifungal and photocatalytic activity of Pithecellobium dulce peel-mediated ZnO nanoparticles. 127, 43-51.
- [13] Parthiban, C., Sundaramurthy, N.J.I.J.o.I.R.i.S., Engineering, and Technology, (2015). Biosynthesis, characterization of ZnO nanoparticles by using Pyrus pyrifolia leaf extract and their photocatalytic activity. 4(10), 9710-9718.
- [14] Shim, Y.J., Soshnikova, V., Anandapadmanaban, G., Mathiyalagan, R., Perez, Z.E.J., Markus, J., Kim, Y.J., Castro-Aceituno, V., and Yang, D.C.J.O., (2019). Zinc oxide nanoparticles synthesized by Suaeda japonica Makino and their photocatalytic degradation of methylene blue. 182, 1015-1020.
- [15] Rao, S.M., Kotteeswaran, S., and Visagamani, A.M.J.I.C.C., (2021). Green synthesis of zinc oxide nanoparticles from camellia sinensis: Organic dye degradation and antibacterial activity. 134, 108956.
- [16] Hassan, S.S., El Azab, W.I., Ali, H.R., Mansour, M.S.J.A.i.N.S.N., and Nanotechnology, (2015). Green synthesis and characterization of ZnO nanoparticles for photocatalytic degradation of anthracene. 6(4), 045012.
- [17] Rambabu, K., Bharath, G., Banat, F., and Show, P.L.J.J.o.h.m., (2021). Green synthesis of zinc oxide nanoparticles using Phoenix dactylifera waste as bioreductant for effective dye degradation and antibacterial performance in wastewater treatment. 402, 123560.
- [18] Alharthi, F.A., Alghamdi, A.A., Allothman, A.A., Almarhoon, Z.M., Alsulaiman, M.F., and Al-Zaqri, N.J.C., (2020). Green synthesis of ZnO nanostructures using Salvadora Persica leaf extract: applications for photocatalytic degradation of methylene blue dye. 10(6), 441.
- [19] Sadiq, H., Sher, F., Sehar, S., Lima, E.C., Zhang, S., Iqbal, H.M., Zafar, F., and Nuhanović, M.J.J.o.M.L., (2021). Green synthesis of ZnO nanoparticles from Syzygium Cumini leaves extract with robust photocatalysis applications. 335, 116567.
- [20] Raja, A., Ashokkumar, S., Marthandam, R.P., Jayachandiran, J., Khatiwada, C.P., Kaviyarasu, K., Raman, R.G., Swaminathan, M.J.J.o.P., and Biology, P.B., (2018). Eco-friendly preparation of zinc oxide nanoparticles using Tabernaemontana divaricata and its photocatalytic and antimicrobial activity. 181, 53-58.

- [21] Suresh, D., Nethravathi, P., Kumar, M.P., Naika, H.R., Nagabhushana, H., and Sharma, S.J.M.S.i.S.P., (2015). Chironji mediated facile green synthesis of ZnO nanoparticles and their photoluminescence, photodegradative, antimicrobial and antioxidant activities. 40, 759-765.
- [22] Sasi, S., Fasna, P.F., Sharmila, T.B., Chandra, C.J., Antony, J.V., Raman, V., Nair, A.B., Ramanathan, H.N.J.o.A., and Compounds, (2022). Green synthesis of ZnO nanoparticles with enhanced photocatalytic and antibacterial activity. 924, 166431.
- [23] Soto-Robles, C., Luque, P., Gómez-Gutiérrez, C., Nava, O., Vilchis-Nestor, A., Lugo-Medina, E., Ranjithkumar, R., and Castro-Beltrán, A.J.R.i.P., (2019). Study on the effect of the concentration of Hibiscus sabdariffa extract on the green synthesis of ZnO nanoparticles. 15, 102807.
- [24] Chen, L., Batjikh, I., Hurh, J., Han, Y., Huo, Y., Ali, H., Li, J.F., Rupa, E.J., Ahn, J.C., and Mathiyalagan, R.J.O., (2019). Green synthesis of zinc oxide nanoparticles from root extract of Scutellaria baicalensis and its photocatalytic degradation activity using methylene blue. 184, 324-329.



Efficiency analysis of clutch production line stations in the automotive industry using multi-criteria decision-making methods

Adnan Abdulvahitoğlu¹ , Aslı Abdulvahitoğlu^{2#} , İrem Salman³ 

Abstract

Today, companies that best meet customer demands stand out in the competitive landscape. As a result, businesses strive to improve their production processes to achieve timely delivery, high quality, and low cost. Lean manufacturing philosophy, which aims to reduce waste and increase efficiency, has become an effective strategy in achieving these goals. In this study, improvements were made in an automotive company by utilizing lean production techniques. Following these improvements, the efficiency of each station within the production line was evaluated. The new data obtained were analysed using Multi-Criteria Decision Making (MCDM) methods to determine at which station the optimum efficiency increase occurred. Additionally, a model was proposed to identify which stations should be prioritized in future improvement efforts. This model provides a scientific approach to assessing the tangible outcomes of lean manufacturing applications and contributes to the process of continuous improvement.

Keywords: Automotive Industry; Clutch Production; Efficiency; Lean Production; MCDM

¹Mudanya University, Department of Industrial Engineering, 16940 Bursa, Türkiye

ORCID: 0000-0002-2659-6709

²Adana Alparslan Türkeş Science and Technology University, Department of Mechanical Engineering, 01250 Adana, Türkiye

ORCID: 0000-0002-3603-6748

³Feka Automotive, 16140 Bursa, Türkiye

ORCID: 0009-0007-5406-8026

#Corresponding Author:

E-mail: aabdulvahitoglu@atu.edu.tr

Otomotiv endüstrisinde debriyaj üretim hattı istasyonlarının verimliliğinin çok kriterli karar verme yöntemleri ile analizi

Öz

Günümüzde müşteri taleplerini en iyi şekilde karşılayabilen firmalar, rekabet avantajı elde etmektedir. Bu nedenle şirketler; zamanında teslimat, yüksek kalite ve düşük maliyet hedeflerine ulaşabilmek adına üretim süreçlerini sürekli olarak iyileştirmeye çalışmaktadır. Bu hedeflere ulaşmada etkili bir strateji olan yalın üretim felsefesi, israfı azaltarak verimliliği artırmayı amaçlamaktadır. Bu çalışmada, bir otomotiv işletmesinde yalın üretim teknikleri uygulanarak gerçekleştirilen iyileştirmeler ele alınmıştır. Yapılan uygulamalar sonucunda, üretim hattında yer alan her bir istasyonun verimliliği değerlendirilmiştir. Elde edilen yeni veriler, Çok Kriterli Karar Verme (ÇKKV) yöntemleriyle analiz edilerek, verimlilik artışının en fazla hangi istasyonda gerçekleştiği tespit edilmiştir. Ayrıca, gelecekte yapılacak iyileştirme çalışmalarında hangi istasyonlara öncelik verilmesi gerektiğine dair bir model önerisi geliştirilmiştir. Bu kapsamda geliştirilen model, yalın üretim uygulamalarının somut çıktılarla değerlendirilmesine olanak tanımakta ve sürekli iyileştirme sürecine bilimsel bir yaklaşım sunmaktadır.

Anahtar Kelimeler: Otomotiv Sektörü; Debriyaj Üretimi; Verimlilik; Yalın Üretim; ÇKKV

Received: 15/04/2025

Revised: 2/05/2025

Accepted: 21/05/2025

Online Published: 20/06/2025

How to Cite: Abdulvahitoğlu A., Abdulvahitoğlu A. Salman İ., "Efficiency Analysis of Clutch Production Line Stations in the Automotive Industry Using Multi-Criteria Decision-Making Methods" Adana Alparslan Türkeş Science and Technology University Journal of Science, **1** (1): 28-39 (2025).

1. Introduction

The automotive industry is defined as a branch of industry encompassing the design, development, production, and marketing of motor vehicles. Globally, this sector is regarded as one of the fundamental drivers of economic growth in industrialized countries and represents one of the highest export volume sectors in Türkiye. The Turkish automotive industry operates in a highly competitive environment driven by price, performance, and particularly comfort, in line with technological advancements. Today, rapid changes in global economic dynamics, technology-driven transformations, and the increasing diversity of customer expectations have intensified competition across many sectors, including the automotive industry [1]. The key to success in this competitive environment lies in the ability to provide the most suitable, timely, high-quality, and cost-effective solutions to meet customer demands. High-quality production alone is no longer sufficient; timely delivery, efficient resource utilization, and cost minimization have also become strategically important for businesses [2].

In this context, it has become inevitable for businesses to restructure their customer-focused production processes and turn to various production strategies in order to gain competitive advantage. However, traditional production methods do not always produce the desired results; fundamental problems such as waste, inefficiency and quality problems are among the main difficulties faced by companies [3]. The lean production system, which was developed as a solution to these problems and is widely applied in many sectors today, offers businesses the opportunity to make their production processes more efficient, flexible and customer-focused [4]. The lean production approach dates its origins to the Toyota Production System (TPS), developed in Japan in the mid-20th century. TPS aims to systematically eliminate all activities that do not create added value in the production process, i.e. waste. The success of the system has enabled the lean production philosophy to be adopted not only in Japan but also worldwide and to spread internationally since the 1990s [5]. Subjects such as optimization of automobile clutch and power transmission units [6], clutch damping studies in passenger cars [7], improvement of clutch diaphragm springs [8], temperature analysis in dry friction clutches [9], effect of clutch systems on vehicle comfort [10], materials used in clutch disc production [11], surface hardness analysis in clutch manufacturing [12], optimization of clutch engagement process [13], design of clutch testing apparatus [14], safety effects of dry clutches [15], use of composite materials in clutch manufacturing [16], future clutch systems [17], design of aluminium clutch housing molds [18], improvement of thermo-mechanical properties of clutches [19], clutch cover design in light commercial vehicles [20] and clutch and shuttle lever locking mechanisms in tractors [21], have been studied in detail in the literature. In addition, studies on the effects of the lean manufacturing system on the socio-economic structures of enterprises [22], the contributions of lean manufacturing applications to firm profitability and efficiency [23] and the applicability of lean manufacturing techniques in logistics activities [24] reveal the multi-dimensional effects of this approach.

Although many theses have been written on clutch systems in Türkiye, it is noteworthy that these studies have not been widely disseminated through national and international academic publications. In this context, a bibliometric visualization conducted using VOSviewer software based on studies published in the Web of Science database is illustrated in Figure 1; related publications are widely dispersed and cover a broad thematic range. This dispersion reflects the complex structure of the automotive industry and the presence of numerous sub-sectors, resulting in a fragmented and multi-dimensional research landscape. The visualization results indicate that, to date, there appears to be no comprehensive study in the literature that holistically addresses lean manufacturing, clutch systems, and MCDM methods together.

Therefore, in this study, the improvement results of bottlenecks and waste elements identified using a lean production tool, aimed at increasing efficiency in the clutch disc production line of an automotive company, were analyzed using MCDM methods. In the first stage of the study, the theoretical foundation of the lean production philosophy was explained. In the second stage, the clutch production process was discussed. In the third stage, MCDM methods were introduced. In the fourth stage, the efficiency of the stations—where improvement works had been implemented based on the lean production philosophy—was analysed using MCDM methods. In the final stage, the findings were evaluated and various conclusions and recommendations were provided. The stages of the study are illustrated in Figure 2 below.

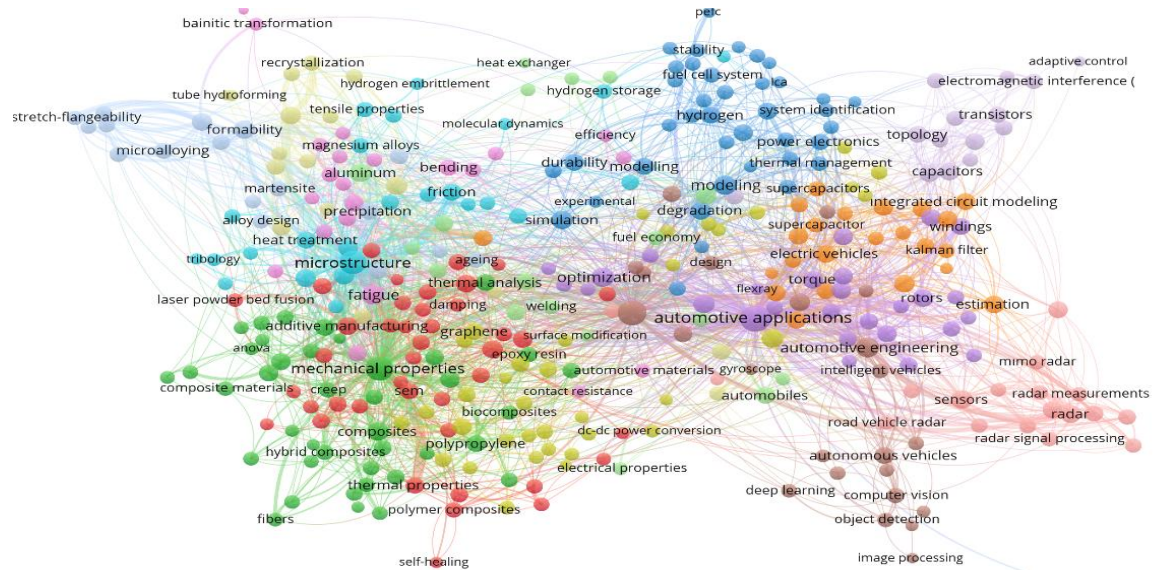


Figure 1. Visualization Showing Lack of Integrated Studies on Lean Production, Clutch Systems, and MCDM (created by the authors).

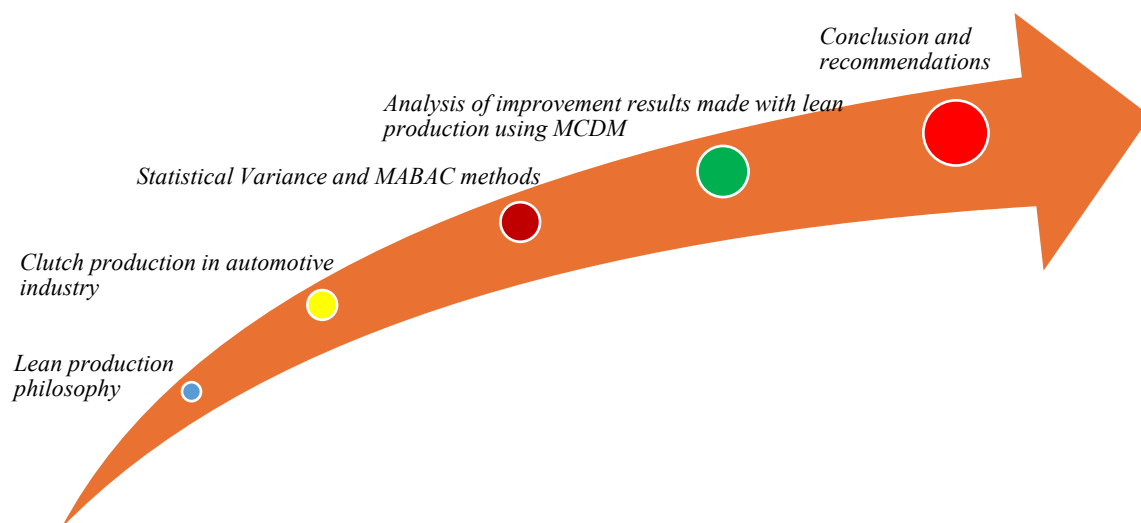


Figure 2. Stage of the study.

2. Methods

In the automotive industry, the application of lean manufacturing techniques in the clutch production line has strategic importance in terms of increasing process efficiency, reducing waste and reducing production costs. Especially by integrating lean manufacturing tools such as 5S, Kaizen, Value Stream Mapping (VSM) and Kanban, bottlenecks in the production line can be determined, cycle times can be optimized and issues such as inventory management can be carried out more effectively. The results of these applications can be evaluated with MCDM methods in order to analyse the effects of lean manufacturing processes on production performance in a systematic and measurable way. In this study, the improvement results of the stations in the clutch production line according to certain criteria were analysed using the Statistical Variance Integrated MABAC method and the efficiency levels of the stations were compared.

Thus, the MCDM approach has made it possible to prioritize among improvement criteria and to optimize the production process. In this respect, lean manufacturing practices not only contribute to increased operational efficiency, but also support strategic planning by providing a quantitative basis for decision-making processes. Such approaches play a significant role in the restructuring of production processes in both developed and developing countries. In this context, a bibliometric visualization conducted using VOSviewer software based on

studies published in the Web of Science database illustrates the countries in which research focusing on lean manufacturing and clutch production is concentrated (Figure 3).

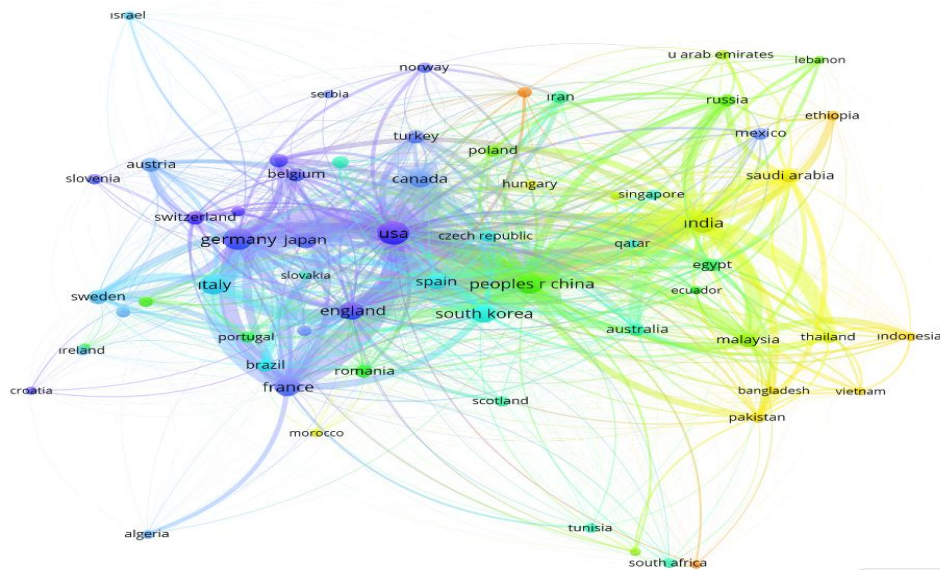


Figure 3. Countries with studies on lean manufacturing, clutch production (Created by the authors).

2.1 Lean production

Lean production is a holistic production approach that aims to prioritize processes that create value for the customer and systematically eliminate activities that do not create value and therefore cause waste. Waste covers all elements other than the minimum equipment, materials, time and labor required for production and is classified under seven headings: overproduction, waiting, transportation, excess inventory, unnecessary process, unnecessary movement, and product defects [25]. Reducing these wastes makes it possible to design production processes with lower costs, fewer errors, and fewer resource usage [26, 27]. The lean production approach is not limited to physical production; it also aims to analyse and eliminate delays in information flow, excess stock, and unnecessary process steps. Thus, businesses achieve a significant competitive advantage by reducing costs and increasing efficiency and quality [28].

The basic components of lean production include encouraging employee participation and adopting a culture of continuous improvement (Kaizen). This approach provides a holistic transformation in many areas, from production to supply chain management, from customer relations to quality control and human resources. In particular, the integration of suppliers into the lean production system creates direct gains such as improvement in product quality, reduction in costs, and shortening in delivery times, while also strengthening cooperation between businesses [29].

The flexibility offered by lean production enables businesses to respond quickly and effectively to changing market conditions; this creates a strategic advantage, especially in sectors such as automotive, which are sensitive to technological transformation and customer demands. In this context, lean production is not only a production model, but also considered one of the fundamental building blocks of contemporary business management [30]. As a result, the lean production approach aims to increase efficiency, reduce costs, and improve quality by preventing waste in all processes from customer order to shipment; thus, it contributes to companies gaining long-term competitive advantage [31]. There are eleven lean production techniques. These are [22];

- i. Just In Time (JIT)
- ii. Value Stream Mapping
- iii. Pull System (Kanban)
- iv. Continuous Improvement (Kaizen)
- v. Error-Proofing Systems (Poka-Yoke)
- vi. 5S
- vii. Balanced Production (Heijunka)
- viii. Jidoka (Automation)
- ix. Work and Line Balancing (Yamazumi)

- x. Total Productive Maintenance
- xi. Single Minute Exchange of Dies (SMED)

In this study, the improvement results of a clutch production facility were analysed with MCDM techniques by applying Value Stream Mapping (VSM). As a result of the analysis, a model was proposed in which the stations that should be addressed first for future improvements in the clutch production line were determined.

2.2 Clutch production

The clutch is a basic transmission organ that provides the connection between the engine and the transmission. It enables the vehicle to be started, stopped, and its speed to be changed depending on the driver's request. The tasks of clutch systems [32];

- i. Allowing gear changes while the vehicle is in motion,
- ii. Transferring torque to the transmission,
- iii. Ensuring a smooth start by reducing torsional vibrations and irregularities coming from the engine,
- iv. Equalizing the engine and transmission output speeds by regulating the torque flow.

In order to change gears, the engine must be separated from the transmission; this process is undertaken by the clutch. It ensures that the engine and gearbox with different rotational speeds are reunited in a harmonious way and dissipates the heat generated in a way that will not harm it. It also acts as a safety valve that protects the transmission against sudden and high torques.

When the clutch operates, relative movements occur between the internal components and friction forces occur as a result of these movements. The effect created by these forces is called hysteresis and is controlled by friction. Hysteresis washers increase driving comfort by damping vibrations coming from the transmission [33].

The clutch provides a connection between 2 shafts that transfer motion and torque, which can separate the drive shaft from the driven shaft if desired [34]. Clutch systems allow the operation of high inertia loads with small forces and are also widely used in all types of production machines [35]. The clutch system is less complex than the engine and transmission and consists of 3 main components and 2 auxiliary components (Figure 4). These are [34];

- i. Clutch Pressure Plate
- ii. Clutch Disc
- iii. Clutch Bearing
- iv. Flywheel (Auxiliary)
- v. Clutch Fork (Auxiliary)

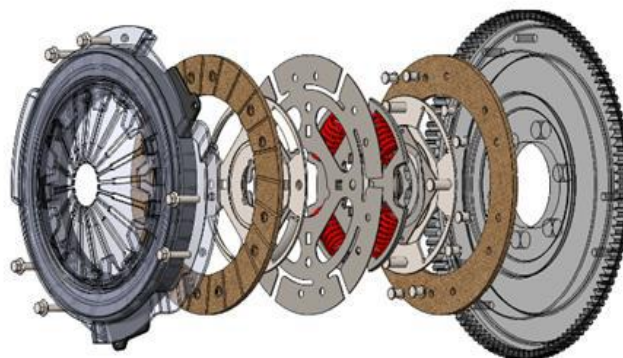


Figure 4. Clutch system [34].

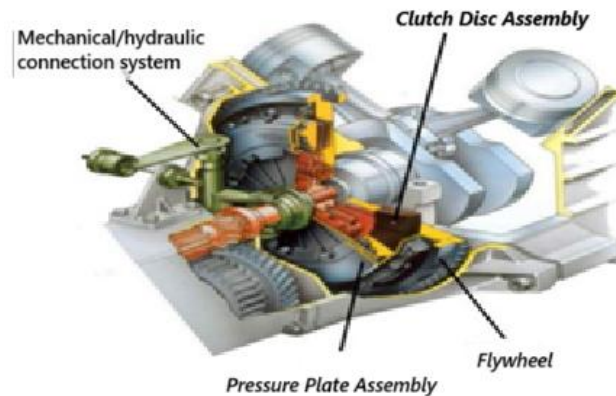


Figure 5. Parts of the clutch system [10].

The clutch system is the system that provides separation and engagement between the engine and the gearbox in manual vehicles. The parts in the clutch system, which protect the gearbox by preventing the irregular vibrations coming from the engine from being dampened and transferred to the gearbox during engagement, have different functions within themselves. The main parts that make up the system, the Flywheel, the Pressure Assembly and the Disc Assembly, are shown in Figure 5 as a whole [10].

Clutches are a fundamental element in the transmission systems of automobiles and play a critical role in the efficient and sustainable operation of vehicles. Clutches, which act as an intermediary between the engine and the gearbox, facilitate the starting, braking and gear changing processes of the vehicle by enabling the engagement and disengagement of the transmission systems; they also contribute to the protection of the system components [36]. The importance of this component cannot be ignored, because poor clutch performance can lead to premature failure of other parts of the transmission system, as well as pose safety risks for the driver and passengers [37]. In today's context, where technological developments are accelerating and demands in engineering and industry are increasing, research and development of materials and production processes are becoming more important than ever. Modern materials must meet high performance and durability requirements; it is also important that they are produced in compliance with environmental and safety standards [11]. Therefore, in this study, clutch production line stations are considered holistically, and the results of improvements made in a company in Bursa are shown in Table 1.

Table 1. Results of line improvement in disc production [38].

Assembly Line	Number of operator	Cycle time (minute)	Operation time (minute)	Downtime (minute)	Defective part count	Die change time (minute)	Production Quantity	Number of die changes	Overall Equipment Effectiveness (OEE)(%)
Criterion Type	min	min	min	min	min	min	max	max	max
Op10 Disc	1	64	1105	5	1	25	1025	2	86.60
Op20 Disc	1	45	1111	29	2	20	1024	2	60.77
Op30 Disc	0.5	45	1132	8	4	20	1022	2	60.54
Op40 Disc	1	42	1073	7	3	30	1018	2	56.33
Op10 Disc Assembly	0	35	1047	33	2	20	1015	3	46.85
Op20 Disc Assembly	1	25	1118	22	3	20	1013	2	33.37
Firewall	1	56	1251	9	1	0	1010	0	74.67
Pressure Plate	1	70	1253	7	0	0	1009	0	93.33
Packaging									

2.3 Multi- Criteria Decision Making

In the decision-making process, the number of alternatives and the factors influencing the selection of these alternatives play a significant role. As the number of alternatives and influencing factors increases, the process becomes more complex, thus requiring the use of MCDM methods to reach optimal solutions and make the most accurate decisions. There are nearly 200 MCDM methods available in the literature [39]. In MCDM methods, the decision-making process typically follows the sequence of steps illustrated in Figure 6. The data presented in Table 1 are objective in nature and do not require the intervention of decision-makers; therefore, the Standard Deviation method was used for weighting. The alternatives were ranked using the MABAC method, which is one of the most recent MCDM techniques. This method was preferred due to its computational simplicity, sensitivity to decision-makers' evaluations, and ability to provide direct comparison with the ideal performance.

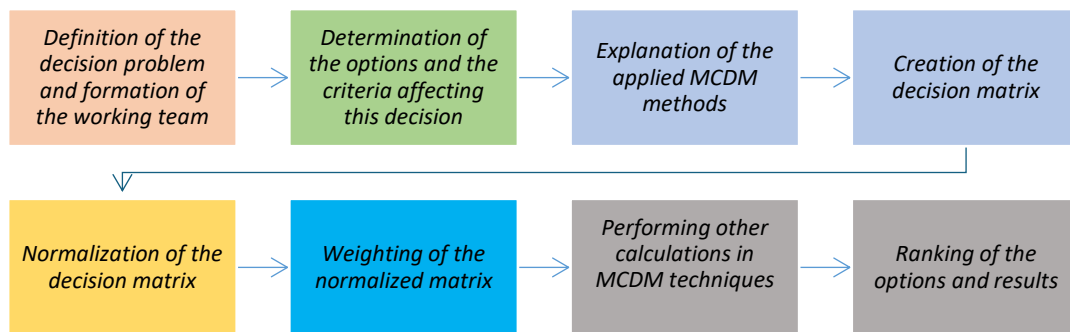


Figure 6. Multi-Criteria Decision-Making (MCDM) Process [40].

2.3.1. Statistical variance method

The Statistical Variance (SV) method, also known as the Variance Method, was developed by Rao and Patel in 2010 to determine the objective weights of criteria [41]. The calculation steps of the SV method are outlined below [42].

Step 1. Construction of the decision matrix. The decision matrix X of size $(m \times n)$ is constructed as shown in Equation (1). The element x_{ik} represents the values in the decision matrix, where n denotes the alternatives and m represents the criteria.

$$X = \begin{bmatrix} X_{11} & X_{12} & \cdots & X_{1n} \\ X_{21} & X_{22} & \cdots & X_{2n} \\ \vdots & \vdots & \cdots & \vdots \\ X_{m1} & X_{m2} & \cdots & X_{mn} \end{bmatrix} \quad (1)$$

Step 2. Normalization of the decision matrix. Criteria with a maximization direction are normalized using Equation (2), while criteria with a minimization direction are normalized using Equation (3).

$$n_{ij}^* = \frac{x_{ij} - x_j^{\min}}{x_j^{\max} - x_j^{\min}} \quad (2)$$

$$n_{ij}^x = \frac{x_j^{\max} - x_{ij}}{x_j^{\max} - x_j^{\min}} \quad (3)$$

Step 3. Calculation of the variance values of the criteria. The variance (σ^2) value for each criterion is calculated using Equation (4). In the equation, V_j represents the variance of the data corresponding to the j^{th} criterion.

$$V_j = \left(\frac{1}{n}\right) \sum_{i=1}^n (a_{ij}^* - \bar{a}_{ij}^*)^2 \quad (4)$$

Step 4. Calculation of the weights of the criteria. The weight of each criterion is determined using Equation (5).

$$W_{jSV} = \frac{V_j}{\sum_{i=1}^m V_j} \quad (5)$$

2.3.2. MABAC method

MABAC (Multi-Attributive Border Approximation Area Comparison) is one of the Multi-Criteria Decision-Making (MCDM) methods. Developed by Pamučar and Ćirović in 2015, the MABAC method is based on evaluating decision alternatives by considering the distances of their criterion functions from the border approximation area. The MABAC method is implemented using the following steps [43-45].

Step 1. Constructing the decision matrix. Once the problem is defined, the alternatives and criteria related to the problem are used to construct the decision matrix using Equation (6).

$$X = \begin{bmatrix} x_{11} & x_{12} & \cdots & x_{1n} \\ x_{21} & x_{22} & \ddots & x_{2n} \\ \vdots & \vdots & \ddots & \vdots \\ x_{m1} & x_{m2} & \cdots & x_{mn} \end{bmatrix} \quad (6)$$

Step 2. Normalization of the decision matrix: For benefit-oriented criteria, Equation (7) is used, while for cost-type criteria, Equation (8) is applied.

$$r_{ij} = \frac{x_{ij} - x_j^{\min}}{x_j^{\max} - x_j^{\min}} \quad (7)$$

$$r_{ij} = \frac{x_j^{\max} - x_{ij}}{x_j^{\max} - x_j^{\min}} \quad (8)$$

Step 3. Calculation of the weighted normalized matrix: Using the weights determined for each criterion through the SV method, the normalized values are weighted as shown in Equation (9).

$$V_{ij} = W_j * (1 + r_{ij}) \quad (9)$$

Step 4. Obtaining the border proximity matrix. The border proximity area matrix (G) is obtained using Equations (10) and (11).

$$g_i = (\prod_{i=1}^m V_{ij})^{1/m} \quad (10)$$

$$G = [g_i]_{1 \times n} \quad (11)$$

Step 5. Determining the distances of the alternatives from the border proximity values. These distances are calculated using Equations (12) and (13).

$$Q = (v_i - G) = \begin{bmatrix} v_{11} - g_1 & v_{12} - g_2 & \cdots & v_{1n} - g_n \\ v_{21} - g_1 & v_{22} - g_2 & \cdots & v_{2n} - g_n \\ \vdots & \vdots & \ddots & \vdots \\ v_{m1} - g_1 & v_{m2} - g_2 & \cdots & v_{mn} - g_n \end{bmatrix} = \begin{bmatrix} q_{11} & q_{12} & \cdots & q_{1n} \\ q_{21} & q_{22} & \cdots & q_{2n} \\ \vdots & \vdots & \ddots & \vdots \\ q_{m1} & q_{m2} & \cdots & q_{mn} \end{bmatrix} \quad (12)$$

$$A_i \in \begin{cases} G^+ & \text{if } q_{ij} > 0 \\ G & \text{if } q_{ij} = 0 \\ G^- & \text{if } q_{ij} < 0 \end{cases} \quad (13)$$

Step 6. Ranking of the alternatives. The alternatives specified in the decision matrix X are calculated using Equation (14) and then ranked in descending order.

$$S_i = \sum_{j=1}^n q_{ij} \quad (14)$$

3. Results and Discussion

There are a total of 8 stations in the clutch production line. The results obtained from improvements made using lean manufacturing techniques through the VSM are presented in Table 1. In Table 1, the improvement results are listed under 9 main headings. In this study, the significance level of each improvement result will first be calculated using the Statistical Variance method. Then, using the obtained significance levels, the performance values of the 8 stations on the production line will be determined through a comparative analysis conducted with the MABAC method. The normalized version of the data in Table 1 using the Statistical Variance method is shown below in Table 2.

Table 2. Normalized Matrix in the Statistical Variance Method

<i>Assembly Line</i>	Number of operator	Cycle time (minute)	Operation time (minute)	Downtime (minute)	Defective part count	Die change time (minute)	Production Quantity	Number of die changes	Overall Equipment Effectiveness (OEE)(%)
Criterion type	min	min	min	min	min	min	max	max	max
Op10 Disc	0	0.133	0.718	1	0.75	0.167	0.667	1	0.888
Op20 Disc	0	0.556	0.689	0.143	0.5	0.333	0.667	0.938	0.457
Op30 Disc	0.5	0.556	0.587	0.893	0	0.333	0.667	0.813	0.453
Op40 Disc	0	0.622	0.874	0.929	0.25	0	0.667	0.563	0.383
Op10 Disc Assembly	1	0.778	1	0	0.5	0.333	1	0.375	0.225
Op20 Disc Assembly	0	1	0.655	0.393	0.25	0.333	0.667	0.25	0
Firewall	0	0.311	0.01	0.857	0.75	1	0	0.063	0.689
Pressure Plate Packaging	0	0	0	0.929	1	1	0	0	1

As a result of the calculations performed using the Statistical Variance method, the weights of the performance evaluation criteria for the clutch production line stations are shown below in Table 3.

Table 3. Performance Evaluation Criteria and Weights for Clutch Production Line Stations.

Criteria	Number of operator	Cycle time (minute)	Operation time (minute)	Downtime (minute)	Defective part count	Die change time (minute)	Production Quantity	Number of die changes	Overall Equipment Effectiveness (OEE)(%)
Weight	0.1177	0.0934	0.1166	0.1367	0.0911	0.1144	0.1063	0.1291	0.0946

After the weights of each performance criterion in the clutch production line were determined, the efficiency of the eight production stations was analysed comparatively using the MABAC method. The normalized decision matrix used in the MABAC method is presented in Table 4.

Table 4. Normalized Matrix in the MABAC Method

<i>Assembly Line</i>	Number of operator	Cycle time (minute)	Operation time (minute)	Downtime (minute)	Defective part count	Die change time (minute)	Production Quantity	Number of die changes	Overall Equipment Effectiveness (OEE)(%)
Criterion type	min	min	min	min	min	min	max	max	max
Criterion weight	0.118	0.093	0.117	0.137	0.091	0.114	0.106	0.129	0.095
Op10 Disc	0	0.133	0.718	1	0.75	0.167	0.667	1	0.888
Op20 Disc	0	0.556	0.689	0.143	0.5	0.333	0.667	0.938	0.457
Op30 Disc	0.5	0.556	0.587	0.893	0	0.333	0.667	0.813	0.453
Op40 Disc	0	0.622	0.874	0.929	0.25	0	0.667	0.563	0.383
Op10 Disc Assembly	1	0.778	1	0	0.5	0.333	1	0.375	0.225
Op20 Disc Assembly	0	1	0.655	0.393	0.25	0.333	0.667	0.25	0
Firewall	0	0.311	0.01	0.857	0.75	1	0	0.063	0.689
Pressure Plate Packaging	0	0	0	0.929	1	1	0	0	1

After the processes indicated in the other stages of the MABAC method (formulas (6)–(14)) were carried out, the scores and rankings of each production line station were determined, as shown in Table 5 below. The stations ranked as the top three with the highest performance were stations 6, 7, and 8, respectively.

Table 5. MABAC Scores and Performance Ranking of Clutch Production Line Stations

Number	Line station	MABAC Score	MABAC Score	OEE ranking
1	Op10 Disc	0.116959	8	2
2	Op20 Disc	-0.01676	4	4
3	Op30 Disc	0.070679	6	5
4	Op40 Disc	0.002072	5	6
5	Op10 Disc Assembly	0.079277	7	7
6	Op20 Disc Assembly	-0.09984	1	8
7	Firewall	-0.08412	2	3
8	Pressure Plate Packaging	-0.06037	3	1

As a result of lean manufacturing, the ranking of the stations in the production line based on the overall equipment effectiveness (OEE) values showed that the top three stations were station 8, station 1, and station 7. As seen here, the total equipment effectiveness obtained through the lean manufacturing process evaluates each station in the production line individually. However, when all processes are evaluated as a whole using MCDM (Multi-Criteria Decision Making), the results change. The key observation here is that, when considering the production line as a whole, the stations with the lowest performance according to the MCDM evaluation are identified. These stations, in order from the lowest performance, are station 1, station 5, and station 3. In the subsequent lean manufacturing study, focusing on improvements specifically at these three stations will contribute to achieving a holistic performance improvement in clutch production. The analysis was conducted using Microsoft Excel.

4. Conclusions

In today's competitive business world, businesses that can best meet customer expectations stand out. In this direction, companies aim to deliver their products and services on time, with high quality and at low cost. Lean production, which is an effective method for achieving these goals, is a strategic approach that aims to increase process efficiency by reducing waste. VSM, one of the lean production techniques, analyses the production process from beginning to end, visualizes waste elements and improves processes. VSM, which visualizes the production flow through special symbols, provides holistic information about cycle times, stock levels, transitions between stations and quality control points.

In this study, the production process of an automotive sub-industry company producing clutch discs in Bursa province was analysed with lean production techniques. The clutch system is a critical component in the automobile's power transmission mechanism and undertakes an important function in terms of driving safety, comfort, fuel efficiency and vehicle life by controlling the torque transfer between the engine and transmission. The quality and precision production of this system, which ensures that the engine continues to operate especially during gear changes, has become even more critical with the developing automatic and hybrid technologies.

Lean production aims not only to increase operational efficiency, but also to systematically eliminate activities that do not create value and to adopt a culture of continuous improvement with employee participation. However, as the findings of the study reveal, the integration of MCDM methods is important to increase the effectiveness of lean production applications. MCDM allows for the numerical and systematic analysis of the improvements made, and ensures that which applications are more effective or ineffective and that resources are directed to priority areas.

In conclusion, the lean production approach integrated with MCDM contributes to the optimization of production processes; it provides not only increased efficiency but also a scientific basis for strategic decision-making processes. This approach can be re-applied by changing both the lean production technique used and the decision-making method used in the analysis; the results obtained can be evaluated with sensitivity analysis. Thus, businesses can develop more effective improvement strategies in order to achieve maximum efficiency, and decision support mechanisms can be provided to managers.

Authors' Contributions

AA: Conceptualization, Methodology, Software, Validation, Writing- Original Draft. **AA:** Writing - Review & Editing, Visualization, Validation. **İS:** Data curation, Writing- Original Draft.

Declaration of Ethical Standards

The author(s) of this article declare that the materials and methods used in this study do not require ethical committee permission and/or legal-special permission.

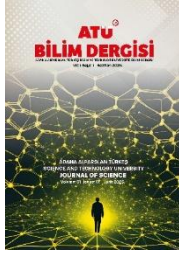
Conflict of Interest

There is no conflict of interest in this study.

References

- [1] Gül, E. C. (2018). İnsan Kaynakları Yönetiminin Bağlamsal (Contextual) Modele Göre Stratejikleşmesi Ve Kalite Anlayışının Aktörler Arası İlişkilere Etkisi. *Uluslararası İktisadi ve İdari Bilimler Dergisi*, 4(1), 70-83.
- [2] Ceran, M. B. (2018). Sürdürülebilir rekabet üstünlüğü sağlamada zaman etkenli faaliyet tabanlı maliyetleme ve tarım makinaları sektöründe uygulanabilirlik düzeyinin belirlenmesi üzerine bir araştırma. Doktora Tezi, Selçuk Üniversitesi Sosyal Bilimler Enstitüsü, Konya.
- [3] Demirkıran, D. (2019). Yalın üretim teknikleri ve Porsche firmasında uygulanması. Y.lisans Tezi, İstanbul Kültür Üniversitesi Lisansüstü Eğitim Enstitüsü, İstanbul.
- [4] Aydın, H. (2009). Yalın üretim sistemi, değer akış haritalama yöntemi ve yalın üretim sisteminin çalışanlara etkileri. Doktora tezi, Marmara Üniversitesi Fen Bilimleri Enstitüsü, İstanbul.
- [5] Solding, P., & Gullander, P. (2009). Concepts for simulation based value stream mapping. In *Proceedings of the 2009 Winter Simulation Conference (WSC)*, 2231-2237, IEEE.
- [6] Ozansoy, O. (2015). Multi-objective optimization of dynamic behaviour of automotive clutch system and power transmission. Doktora Tezi, İTÜ Fen Bilimleri Enstitüsü, İstanbul.
- [7] Avcı, M. (2022). Binek araçlarda debriyajın titreşim sönümlleme performansının iyileştirilmesi ve prototip üretimi. Y.lisans Tezi, Uludağ Üniversitesi, Fen Bilimleri Enstitüsü, Bursa.
- [8] Özbakiş, M. (2008). Debriyaj sistemlerinde kullanılan diyafram yayların karakteristiğinin incelenmesi ve optimizasyonu. Y.lisans Tezi, Dokuz Eylül Üniversitesi, İzmir.
- [9] Abdullah, O. I., & Schlattmann, J. (2012). Finite element analysis of temperature field in automotive dry friction clutch. *Tribology in Industry*, 34(4), 206.
- [10] Dündar, A. (2022). Debriyaj sistemlerinde yastıklamalı yay üretim prosesinin araç konforuna etkisinin incelenmesi. Y.lisans Tezi, Uludağ Üniversitesi, Fen Bilimleri Enstitüsü, Bursa.
- [11] Neculescu, D. A., Ciurdas, M., & Robu, A. Studies And Research On The Materials Used In The Manufacture Of Clutch Discs. *U.P.B. Sci. Bull., Series B*, 86(4), 269-280.
- [12] Gavaskar, S. S., Karthick, K., & Bibin, C. (2021). Statistical analysis on hardness of clutch facing at various stages in clutch face manufacturing. *Materials Today: Proceedings*, 46, 3730-3734.
- [13] Garofalo, F., Glielmo, L., Iannelli, L. & Vasca, F., (2002). Optimal tracking for automotive dry clutch Engagement. *IFAC Proceedings Volumes*, 35(1), 367-372.
- [14] Lu, Y., Guo, B., Fan, W., & Jin, L. (2011, August). Design and Realization of Testing and Analyzing Apparatus for Automobile Clutch. In *2011 Second International Conference on Digital Manufacturing & Automation* (pp. 381-384). IEEE.
- [15] Pourgol-Mohammad, M., Hejazi, A., Soleimani, M., Ghasemi, P., Ahmadi, A., & Jalali-Vahid, D. (2017). Design for reliability of automotive systems; case study of dry friction clutch. *International Journal of System Assurance Engineering and Management*, 8, 572-583.
- [16] Gaikwad, P. B., Girme, S. R., Bagal, P. N., Raut, N. N., & RM, K. (2017). A review on alfa composite material for automotive clutch plate application. *JournalNX*, 3(04), 22-26.
- [17] Freitag, J., Gerhardt, F., Hausner, M., & Wittmann, C. (2010, April). The clutch system of the future. In *Proc. 9th Schaeffler Symp* (pp. 1-10).
- [18] Jeong, S. I., Jin, C. K., Seo, H. Y., Kim, J. D., & Kang, C. G. (2016). Mold structure design and casting simulation of the high-pressure die casting for aluminum automotive clutch housing manufacturing. *The International Journal of Advanced Manufacturing Technology*, 84, 1561-1572.
- [19] Çakmak, T. (2018). Taşıtlarda kullanılan debriyaj sistemlerinin termo-mekanik özelliklerinin iyileştirilmesi. Y.lisans Tezi, Uludağ Üniversitesi Fen Bilimleri Enstitüsü, Bursa.

- [20] Köprübaşı, U. (2024). Hafif ticari araç debriyaj kapağının optimum tasarımı. Y.lisans Tezi, Uludağ Üniversitesi Fen Bilimleri Enstitüsü, Bursa.
- [21] Çakır, Z., Kullukçu, A., Karayel, D., Atalı, G., & Özkan, S. S. (2018). Kabinli Traktörlerde Çubuklu Debriyaj ve Direksiyon Altı Shuttle Kolunun Kilitleme Mekanizmasının Tasarımı ve Analizi. *Academic Perspective Procedia*, 1(1), 458-466.
- [22] Etçi, F., & Terzi, A. (2024). Yalın Üretim Tekniklerinin İşletmelerin Sosyo-Ekonomik Boyutları Üzerindeki Etkileri Ve Sürdürülebilir Maliyet Muhasebesi Perspektifinden İncelenmesi. *Uluslararası Muhasebe ve Finans Araştırmaları Dergisi*, 6(1), 1-18.
- [23] Çetindaş, A. (2024). Yalın üretimin maliyetler ve firma performansı üzerine etkisi. *Akademik Araştırmalar ve Çalışmalar Dergisi (AKAD)*, 16(30), 256-264.
- [24] Uçar, A., & Şirin, B. T. (2024). İç lojistik faaliyetlerinde yalın tekniklerin kullanılması ve bir uygulama. *Black Sea Journal of Engineering and Science*, 7(3), 423-435.
- [25] Taj, S. (2008). Lean Manufacturing Performance İn China: Assessment Of 65 Manufacturing Plants. *Journal of Manufacturing Technology Management*, 19(2), 217-234.
- [26] Wyrwicka, M. K., & Mrugalska, B. (2017). Mirages of lean manufacturing in practice. *Procedia engineering*, 182, 780-785.
- [27] Panwar, A., Jain, R., & Rathore, A. (2015). Lean implementation in Indian process industries--some empirical evidence. *Journal of Manufacturing Technology Management*, 26(1), 131-160.
- [28] Sarıkaya, H. A., Soydemir, E. K., Sardaş, B., Çayır Ervural, B., et al. (2022). Bisküvi Üretim Hatlarında Hazırlık Sürelerinin Azaltılmasına Yönelik Yalın Üretim ve Smed Uygulaması. *Endüstri Mühendisliği*, 33(2), 413-439.
- [29] Chun Wu, Y. (2003). Lean manufacturing: a perspective of lean suppliers. *International Journal of Operations & Production Management*, 23(11), 1349-1376.
- [30] Hines, P., Holweg, M., & Rich, N. (2004). Learning to evolve: a review of contemporary lean thinking. *International journal of operations & production management*, 24(10), 994-1011.
- [31] Yurtseven, Ç., Aydın, D., Ekici, M., Aktepe, S., Yürek, E. E., & Orbak, A. Y. Değer Akış Haritalama Tekniğinin Otomotiv Sektöründe Bir Uygulaması. *Uludağ Üniversitesi Mühendislik Fakültesi Dergisi*, 29(1), 19-36.
- [32] Kabacaoğlu, S., Pekedis, M., & Yıldız, H. (2021). Debriyaj Sistemlerinde Kullanılan Diyafram Yaylarda Formun Yorulma Dayanımı ve Mekanik Karakteristiğe Olan Etkisinin Teorik ve Deneysel Olarak İyileştirilmesi. *Uludağ Üniversitesi Mühendislik Fakültesi Dergisi*, 26(3), 1121-1138.
- [33] Sayaca, S., & Bayram, A., (2008). Debriyajlardaki Histerezis Rondelası İçin Yeni Bir Malzeme Kullanımı ve Parça Geometrisinin Değiştirilmesi. *Uludağ Üniversitesi Mühendislik Fakültesi Dergisi*, 13(1), 129-142.
- [34] Yıldız, Ö., Eş, C., Akbulut, S., Kaymaz, İ. C., Kurt, U., & Çakılı, H. (2022). Debriyaj Diski Dış Ana Sac Batma Prosesinin Etkilerinin İncelenmesi. *Düzce Üniversitesi Bilim ve Teknoloji Dergisi*, 10(5), 127-136.
- [35] Purohit, R., Khitoliya, P., & Koli, D. K., (2014). Design and finite element analysis of an automotive clutch assembly. *Procedia materials science*, 6, 490-502.
- [36] Hajnaye, A., Fernando, J. S., & Sun, Q. (2022). Effects of vehicle driveline parameters and clutch judder on gearbox vibrations. *Proceedings of the Institution of Mechanical Engineers, Part D: Journal of Automobile Engineering*, 236(1), 84-98.
- [37] Cakmak, S., Yildiz, Ö., Kaymaz, İ. C., Kurt, U., & Eş, C. (2022). Alternatif Polimer Esaslı Malzemelerin Debriyaj Diski Stoperine Entegrasyonu. *International Joint Conference on Engineering, Science and Artificial Intelligence-IJCESAI 2022*, 17 Temmuz 2022, Bursa
- [38] Salman, İ. & Yıldız, A., (2024). Değer Akış Haritalama (VSM) Yöntemi Kullanılarak Debriyaj Üretim Sürecinin İyileştirilmesi. *6th International Conference on Applied Engineering and Natural Sciences*, September 25-26, 2024 : Konya, Türkiye.
- [39] Abdulvahitoğlu, A., Vural, D. & Macit, İ., (2024a). Selecting Facility Location of Gendarmerie Search and Rescue (GSR) Units; An Analysis of Efficiency in Disaster Response. *Computers & Industrial Engineering*, 197;110639.
- [40] Abdulvahitoğlu, A., Abdulvahitoğlu, A. & Cengiz, N., (2024b)., A Comprehensive Analysis of Apricot Drying Methods via Multi-Criteria Decision Making Techniques. *Journal of Food Process Engineering*, 47:e14759.
- [41] Yürüyen, A.A., Ulutaş, A. & Özdağoğlu, A., (2023). Lojistik işletmelerinin performansının bir hibrit ÇKKV modeli ile değerlendirilmesi. *BMİJ*, 11 (3): 731-751
- [42] Rao, R. V., & Patel, B. K. (2010). A subjective and objective integrated multiple attribute decision making method for material selection. *Materials & Design*, 31(10), 4738-4747.
- [43] Pamučar, D. & Čirović, G. (2015). The Selection of Transport and Handling Resources in Logistics Centers Using Multi-Attributive Border Approximation Area Comparison (MABAC), *Expert Systems with Applications*, 42(6), 3016-3028.
- [44] Stojanović, I. & Puška, A. (2021). Logistics Performances of Gulf Cooperation Council's Countries in Global Supply Chains, *Decision Making: Applications in Management and Engineering*, 4(1) : 174-193.
- [45] Raj, D., Maity, S. R., & Das, B. (2024). Optimization of process parameters of laser cladding on AISI 410 using MEREC integrated MABAC method. *Arabian Journal for Science and Engineering*, 49(8), 10725-10739.



Determination of changes in antioxidant potential of different plant infusions during storage

Levent Yurdaer Aydemir^{1, #} , Fatma Gizem Akçakaya² 

¹Adana Alparslan Türkeş Science and Technology University, Department of Food Engineering, 01250 Adana, Türkiye

ORCID: 0000-0003-0372-1172

²Adana Alparslan Türkeş Science and Technology University, Department of Food Engineering, 01250 Adana, Türkiye

ORCID: 0000-0002-9866-0159

#Corresponding Author:

E-mail: lyaydemir@atu.edu.tr

Abstract

This study investigated the changes in total phenolic content (TPC), total flavonoid content (TFC), free radical scavenging capacity (FRSC), iron chelating capacity (ICC) values of cinnamon bark, linden flower, linden leaf, sage leaf, and sage stem infusions during storage. The infusions were prepared at 75°C, 85°C, and 95°C for 30 minutes and stored at + 4°C and - 18°C for 30 days. The measurements were carried out on the 5th, 15th, and 30th day of storage. The variations of the determined parameters between the storage days were observed. In cinnamon bark infusion, TPC, TFC, FRSC, ICC values decreased during storage whereas TPC, FRSC, and ICC of sage stem infusions increased. In linden flower, linden leaf, and sage leaf infusions, the common variations were observed as TPC slightly decreased, TFC decreased, FRSC and ICC did not considerably change. These general observations were obtained for every studied infusion and storage temperature of the herbal teas. This study revealed that homemade herbal teas have the potential to be good antioxidants and phenolic sources for human consumption, and they can be stored when they chilled or frozen in the refrigerator.

Keywords: Cinnamon; Linden; Sage; Infusion; Storage; Antioxidant

Depolama sırasında farklı bitki çaylarının antioksidan potansiyelindeki değişikliklerin belirlenmesi

Received: 11/04/2025

Revised: 8/05/2025

Accepted: 9/06/2025

Online Published: 20/06/2025

How to Cite: Aydemir L.Y., Akçakaya F.G. "Determination of changes in antioxidant potential of different plant infusions during storage" Adana Alparslan Türkeş Science and Technology University Journal of Science, 1 (1): 40-49 (2025).

Öz

Bu çalışmada tarçın kabuğu, ıhlamur çiçeği, ıhlamur yaprağı, adaçayı yaprağı ve adaçayı sapı infüzyonlarının (çaylarının) depolama sırasında toplam fenolik içerik (TPC), toplam flavonoid içerik (TFC), serbest radikal süpürme kapasitesi (FRSC) ve demir şelatlama kapasitesi (ICC) değerlerindeki değişimler incelenmiştir. İnfüzyonlar 75°C, 85°C ve 95°C'de 30 dakika süreyle hazırlanmış ve +4°C ve -18°C'de 30 gün süreyle saklanmıştır. Ölçümler depolamanın 5., 15. ve 30. günlerinde gerçekleştirilmiştir. Belirlenen parametrelerin depolama günleri arasındaki değişimleri gözlemlenmiştir. Tarçın kabuğu infüzyonunda TPC, TFC, FRSC, ICC değerleri depolama süresince azalırken, adaçayı sapı infüzyonlarının TPC, FRSC ve ICC değerleri artmıştır. ıhlamur çiçeği, ıhlamur yaprağı ve adaçayı yaprağı infüzyonlarında, TPC hafifçe azalırken, TFC'de belirgin azalışlar tespit edilmiş FRSC ve ICC önemli ölçüde değişmemiştir. Bu genel gözlemlerin, çalışılan bitki tipi ve depolama sıcaklığı için geçerli olduğu görülmüştür. Bu çalışma, ev yapımı bitki çaylarının insan tüketimi için iyi bir antioksidan ve fenolik madde kaynağı olma potansiyeline sahip olduklarını ve soğutulularak veya dondurularak uzun süre saklanabileceklerini ortaya koymuştur.

Anahtar Kelimeler: Tarçın; ıhlamur; Adaçayı; İnfüzyon; Antioksidan; Depolama

1. Introduction

Herbal teas produced by infusion or decoction from aromatic and medicinal plants or spices have been consumed for medicinal purposes flavorings and refreshments since the ancient times [1–4]. Many studies revealed that most of those medicinal herbs or spices showed considerable antioxidant activity by their phenolics, vitamins and alkaloids contents [5, 6]. The antioxidant compounds protect the human metabolism from the effects of free radicals, peroxy radicals, hydroxyl radicals, singlet oxygens and superoxide anions that damages DNA, protein, and lipid structures by oxidation reactions [7–9]. Therefore, those molecules do not show their functions properly, and the risk of occurrence of diseases such as cancer, atherosclerosis, neurodegenerative diseases increases [10, 11]. Due to those beneficial effects, natural phytochemicals extracted from leaves, stems, or flowers of herbal plants have been used for therapeutical purposes. Especially phenolic compounds attracted notable attention, which were mostly found in complex form with other phenolic compounds or other polymeric carbohydrate or lignin in plant tissues. This situation restricts the extraction of phenolic compounds in soluble form from plants. To overcome this problem, thermal extraction processes or organic solvent usage were applied. However, the usage of organic solvents is not preferred for the extracts that would be consumed by humans because of the toxicity of those solvents. Therefore, additional steps are needed to eliminate the solvent from the extract.

The hot water extraction is more appropriate because it softens and disrupts the cellular material and polymeric structures, which allows phenolic compound release to the medium. On the other hand, thermal application could have the detrimental effect on heat labile phenolic compounds that lower the antioxidant capacity of the extracts. Another crucial factor affecting the antioxidant activity of extracts is storage conditions. Especially, the antioxidant potential of herbal infusions might decrease during storage depending on the conditions such as temperature, light, and humidity [12]. For this reason, it is essential to measure the stability of soluble phenolic compounds and antioxidant activity of herbal infusions.

Among those herbal materials, cinnamon (*Cinnamomum verum*), sage (*Salvia officinalis*) and linden (*Tilia cordata*) are the ones mostly used for tea preparation due to their good aroma, pleasant flavor, and health benefits. In the literature, many studies reported their high antioxidant potential sourced from their phenolic compounds [3, 13–16]. However, no studies in the literature were found to have investigated the stability of those infusions at cold and freezing storage conditions, which were the simplest applications for industry and home consumers. For this reason, this study aimed to determine the effects of cold (+4°C) and freezing (-18°C) storage conditions on soluble phenolic content, soluble flavonoid content, free radical scavenging capacity, iron chelating activity, pH, and color properties of cinnamon bark, linden flower, linden leaf, sage leaf, and sage stem infusions prepared at 75, 85, and 95°C.

2. Methods

2.1. Materials

The dry cinnamon bark (*Cinnamomum verum*), sage (*Salvia officinalis*), and linden (*Tilia cordata*) were purchased from local market. Methanol and Folin Ciocalteu reagent were purchased from Merck (Germany), DPPH, ABTS, trolox, FeCl₂, and Ferrozine® were purchased from Sigma Aldrich (the USA), and Na₂CO₃, NaNO₂, and AlCl₃ were purchased from Isolab (Turkey). All other chemicals used in the analysis were at analytical grade.

2.2. Preparation of herbal infusions

The separated leaf and stem part of sage, leaf and flower part of linden, and cinnamon bark were brewed as 5 g herbal sample in 100 ml deionized water at 75 °C, 85 °C and 95 °C. Then infusions were stored at +4°C and -18°C for 30 days and the measurements were conducted at 0th, 6th, 15th and 30th days of storage.

2.3. Total phenolic content (TPC) of herbal infusions

After incubation of 100 µl of the herbal infusion mixed 1000 µl of Folin Ciocalteu reagent (diluted 1/10) for 3 minutes, 800 µl of 7.5% (w/v) Na₂CO₃ was added to the mixture and further incubated for 2 hours in the dark [17].

Then the formed color was measured spectrophotometrically at 765 nm and the results were expressed as gallic acid equivalent as average of 3 parallels (Agilent Carry 60, USA).

2.4. Total flavonoid content (TFC) of herbal infusions:

Firstly, 250 µl herbal infusion diluted with 1000 µl distilled water was mixed with 75 µl 5% (w/v) NaNO₂ and incubated for 5 minutes [18]. Then 75 µl of 10% (w/v) AlCl₃ was added into the mixture and left for 1 minute. The reaction stopped by adding 500 µl 1 mol/L NaOH and mixture was diluted with 600 µl distilled water. The formed color measured spectrophotometrically at 510 nm and the results were expressed in quercetin equivalent as an average of 3 parallels.

2.5. Free Radical Scavenging Capacity (FRSC) of Herbal Infusions:

Firstly, infusions prepared in 50 µl of 80% (v/v) methanol solution were mixed with 1.95 ml DPPH radical solution (the initial absorbance value of the DPPH solution is 0.700 ± 0.010 at 517 nm and left for 30 minutes incubation in the dark [19]. Then the decrease in the absorbance of the mixture was determined and the results were given as Trolox equivalent as average of 3 parallels.

2.6. Iron chelating Capacity (ICC) of Herbal Infusions

Two ml of the appropriate diluted herbal infusions were mixed with 0.1 ml of 1 mmol/L FeCl₂ solution and incubated for 30 before then 0.1 ml of ferrozine was added and further incubated for 10 min [20]. The formed color was measured spectrophotometrically at 562 nm and the results were expressed in EDTA equivalent as average of 3 parallels.

2.7. Color Analyzes and pH measurements of Herbal Infusions

The color analyzes of herbal infusions were made by the colorimeter (Konica Minolta CM-5, Japan) device and the results are given as lightness (L*), redness-greenness (a*), and yellowness-blueness (b*) in 3 parallels. pH of the infusions was measured with pH (WTW inoLab® pH 7110, Germany).

2.8. Statistical analysis

Statistical analyses were carried out using Minitab 18 software. The one-way analysis of variance (ANOVA) of data was evaluated, and significant differences were determined between the results with post-hoc test of Tukey's multiple comparison test at p-value ≤ 0.05 .

3. Results and Discussion

3.1. Storage stability of cinnamon bark infusions

The cinnamon bark infusions prepared at 75 (CB75), 85 (CB85), and 95°C (CB95) had 24349 ± 2513 , 17720 ± 419 , and 20847 ± 1486 µg GA/g dry weight basis TPC, respectively (Figure 1). Although it was expected that the higher process temperature would extract more phenolic compounds from plant cellular material into infusions by softening the structure and disrupting non-covalent interactions such as H-bonding and electrostatic interactions between phenolics and other molecules, some soluble TPC lost were observed by increasing process temperature, which could be associated with heat sensitivity of those phenolic compounds. During 30-day storage at +4°C, significant decrements in TPC were determined in all cinnamon bark infusions. Sixty-eight percent, 63%, and 60% of TPC lost in CB75, CB85, and CB95, respectively. The highest TPC stability (85% remained of initial TPC) was seen in CB75 after 6-day storage. After 15 days, almost 30% of soluble TPC lost in CB75 and CB85 while 18% lost was in CB95. After 6-day storage, between 52 and 66 % TPC lost in all cinnamon infusions was observed at -18°C which was almost equal to TPC lost at +4°C after 30-day storage.

Like TPC, significant reductions were observed in TFC in cinnamon bark infusions during storage at +4°C. The TFC reductions were significant only between 0-6 days and 15-30 days. The highest TFC was determined in CB75

as 113 ± 4 and followed by CB95 as 101 ± 2 and CB85 as 69 ± 3 mg QC/g. Compared to TPC, TFC of CB infusions were highly stable and considerable decrease in values was not observed during 30-day storage. The most stable TFC was in CB75, which remained 86% of initial TFC after 6 days and 82% of initial TFC after 30 days, whereas it was 81% after 6 days and 70% after 30 days in CB85, which was the most unstable infusion. More dramatic decrements were measured in TFC of infusions stored at -18°C . After 30 days, 95% of TPC were lost in all cinnamon infusions. This situation clearly indicated the detrimental effect of freezing and thawing processes on phenolic solubility and stability. On the other hand, an extremely high decrease in TFC values was observed by CB infusions stored at -18°C . It sharply reduced from 113 ± 4 to 17 ± 0 , from 69 ± 3 to 13 ± 1 , and from 101 ± 2 to 13 ± 1 mg QC/g in CB75, CB85, and CB95 infusions, respectively. Similar instability was also determined in TPC of frozen CB infusions, which again proved that freezing and thawing process adversely affected the soluble phenolic content. Even after 6 days incubation, 55%, 29%, and 59% of TFC disappeared in CB75, CB85, and CB95, respectively. However, TFC stability was higher than TPC stability in frozen stored CB infusions. On the other hand, antioxidant activity of CB infusions was preserved at $+4^\circ\text{C}$ for 6 days storage. FRSC values of CB infusions were slightly increased from 83 ± 10 to 106 ± 0 (significant) and from 103 ± 3 to 111 ± 1 $\mu\text{mol Trolox/g}$ (non-significant) in CB75 and CB95, while it was slightly decreased from 92 ± 6 to 84 ± 2 $\mu\text{mol Trolox/g}$ (significant) in CB85, but after 30-day storage, 55%, 84%, and 60% of FRSC were disappeared in CB75, CB85, and CB95, respectively ($P < 0.05$). These reductions were more correlated with TPC reductions.

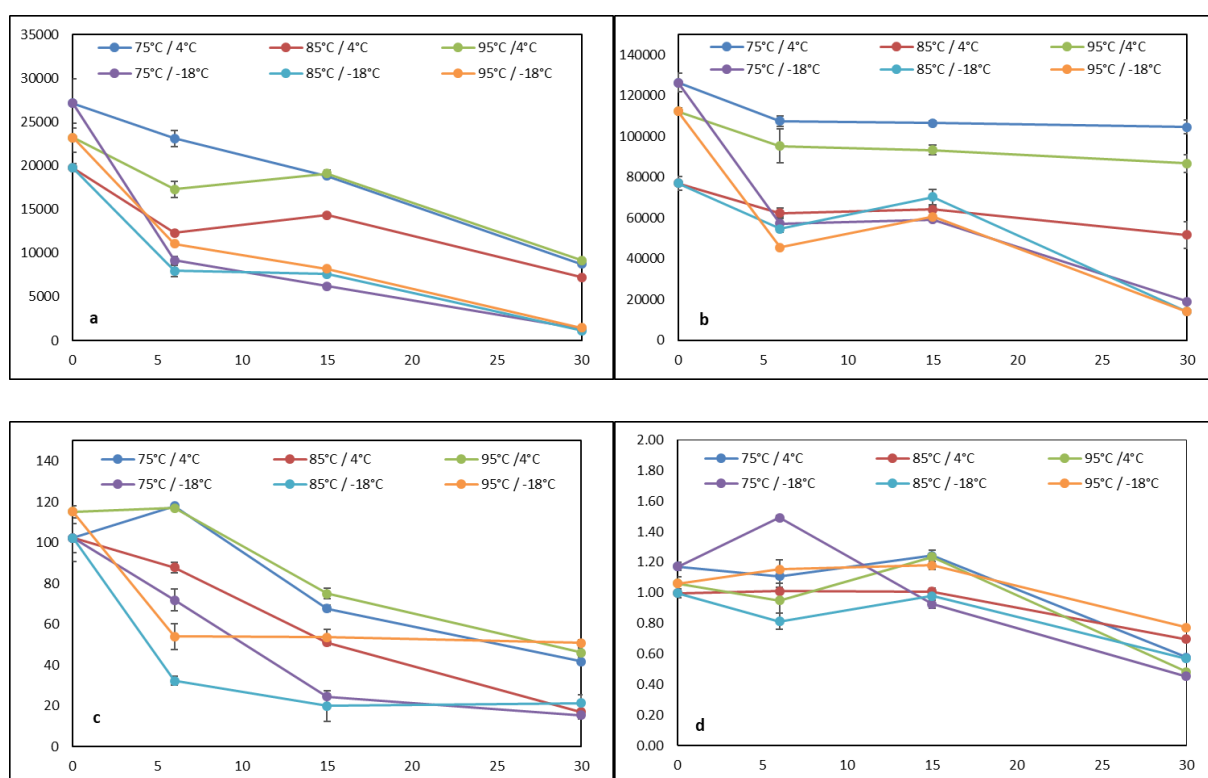


Figure 1. (a) total phenolic content ($\mu\text{g GA/g}$), (b) total flavonoid content ($\mu\text{g quercetin/g}$), (c) free radical scavenging capacity ($\mu\text{mol trolox/g}$), and (d) iron chelating capacity ($\mu\text{mol EDTA/g}$) versus storage days graphs of cinnamon infusions produced at 75°C , 85°C , and 95°C and stored at (+) 4°C and (-) 18°C for 30 days. The results were calculated as dry weight basis.

In frozen infusions, a considerable portion of antioxidants lost after 15-day storage where 74%, 80% and 53% of FRSC were not determined in CB75, CB85, and CB95 infusions, respectively. Interestingly, ICC of CB infusions preserved for 15-day storage at $+4^\circ\text{C}$ and -18°C . However, incredibly low or inconsiderable iron chelating ability was determined in CB infusions. During storage, pH of the CB infusions significantly decreased from 4.93 ± 0.17 to 4.69 ± 0.08 in CB75 and from 4.74 ± 0.04 to 4.60 ± 0.04 in CB 95 at $+4^\circ\text{C}$ and did not significantly change in CB85 as from 4.84 ± 0.06 to 4.89 ± 0.13 ($P < 0.05$).

Significant decreases measured in the pH values of cinnamon teas stored at different temperatures after 30 days ($P < 0.05$). While the pH values did not change or slightly fluctuate in the first 15 days in both storage conditions, it was observed that the teas reached more acidic values when the storage period was extended to 30 days. The pH values were determined between 4.43 ± 0.00 and 4.89 ± 0.13 . This decrement in the solubility or the deterioration of the structure of phenolic components during storage is observed by color measurements. After 6 days, statistically significant increases were detected in L^* values of all stored samples, which indicates that the tea samples were lighter ($P < 0.05$). This trend continued to increase as the storage period increased, which is insignificant ($P < 0.05$). Increases in these L^* values were much greater for cinnamon tea samples stored at -18°C than the samples stored in other conditions. While the a^* redness values measured in the cinnamon tea sample brewed at 75°C were decreased significantly as the storage time increased, the redness was preserved in other stored samples ($P < 0.05$). The b^* values of the samples stored also showed significant increases in all samples with the storage time, but these increases are more for the samples stored at $+4^\circ\text{C}$ ($P < 0.05$).

3.2. Storage stability of linden flower infusions

The linden plant consists of flower, leaf and stem parts, and the leaf and flower parts are brewed together or separately for commercial tea production. Linden flower teas produced by brewing at different temperatures stored at $+4$ and -18°C for 30 days, and total water-soluble phenolic and flavonoid contents, antioxidant capacities, pH and color values were measured (Figure 2). The phenolic component contents of the samples did not show a regular increase or decrease depending on the time and the brewing temperature. While significant decreases were observed in TPCs of linden flower tea stored at $+4^\circ\text{C}$ for the first 15 days, slight increases were observed in 30th day of storage ($P < 0.05$). The highest values for soluble phenolic content at storage are 6th (94% preserved), 30th (93% preserved) and 30th (87% preserved) day for infusions at 75, 85, and 95°C , respectively. At the end of the 30th day, 86% of the phenolic content of the linden flower tea infused at 75°C preserved. This indicates that the phenolic components of linden flower teas maintain their stability for a long-time during storage at $+4^\circ\text{C}$.

The flavonoid content of the samples stored under the same conditions showed a significant decrease with increasing storage time, unlike the TPC values ($P < 0.05$). Interestingly, this decrease in TFC values is inversely proportional to the brewing temperature. The TFC values of linden flower teas brewed at 75, 85, and 95°C and stored at $+4^\circ\text{C}$ decreased by approximately 65%, 56%, and 34%, respectively. This situation indicates that the phenolic components of linden flower teas stored in liquid form at $+4^\circ\text{C}$ partially decreased in their structure during the first 15 days, and after this time, no decrease was observed in solubility. TPC and TFC values of linden flower teas brewed at different temperatures and stored at -18°C by freezing showed significant decreases at the end of 30 days. The loss of phenolic components in tea samples stored by freezing was 2 times higher than tea samples stored as $+4^\circ\text{C}$. TPC values increased or decreased irregularly for 30 days. TFC values of the same samples at the same storage temperature decreased with the increasing number of storage days. Among the linden flower teas stored at -18°C , the minimum decrease in TPC and TFC values was observed in the tea sample produced by brewing at 95°C , and a similar situation is generally valid for samples stored at $+4^\circ\text{C}$.

Antioxidant properties of linden flower teas followed different trends in both parameters. ICC values of teas either preserved their activities or showed significant increases during the 30-day storage period ($P < 0.05$). The highest increases were 35% ($6.58 \pm 0.01 \mu\text{mol EDTA} / \text{g}$) and 21% ($6.08 \pm 0.01 \mu\text{mol EDTA} / \text{g}$) of teas steeped at 75°C for 30 days at $+4^\circ\text{C}$ and -18°C , respectively. FRSC values of linden flower teas also decreased slightly or increased significantly after 30 days of storage. FRSC of teas brewed at high temperatures (85°C and 95°C) increased between 19% and 38% over time, regardless of whether they were stored in at $+4^\circ\text{C}$ and -18°C . Interestingly, the FRSCs of these samples measured after 6 days of storage had the highest values (52%). In the first 6 days, antioxidant substances that can neutralize free radicals can be released into the environment due to depolymerization (Alara et al, 2021).

The pH values of linden flower teas decreased with increasing brewing temperature and storage time, and the samples became more acidic. When the color values were examined, the decrease observed in the L^* values with the increase of the brewing temperature. While no significant changes were determined in a^* values, b^* values increased with the storage time at $+4^\circ\text{C}$. The significant decreases were observed in the b^* values of the samples stored at -18°C on the 6th and 15th day ($P < 0.05$).

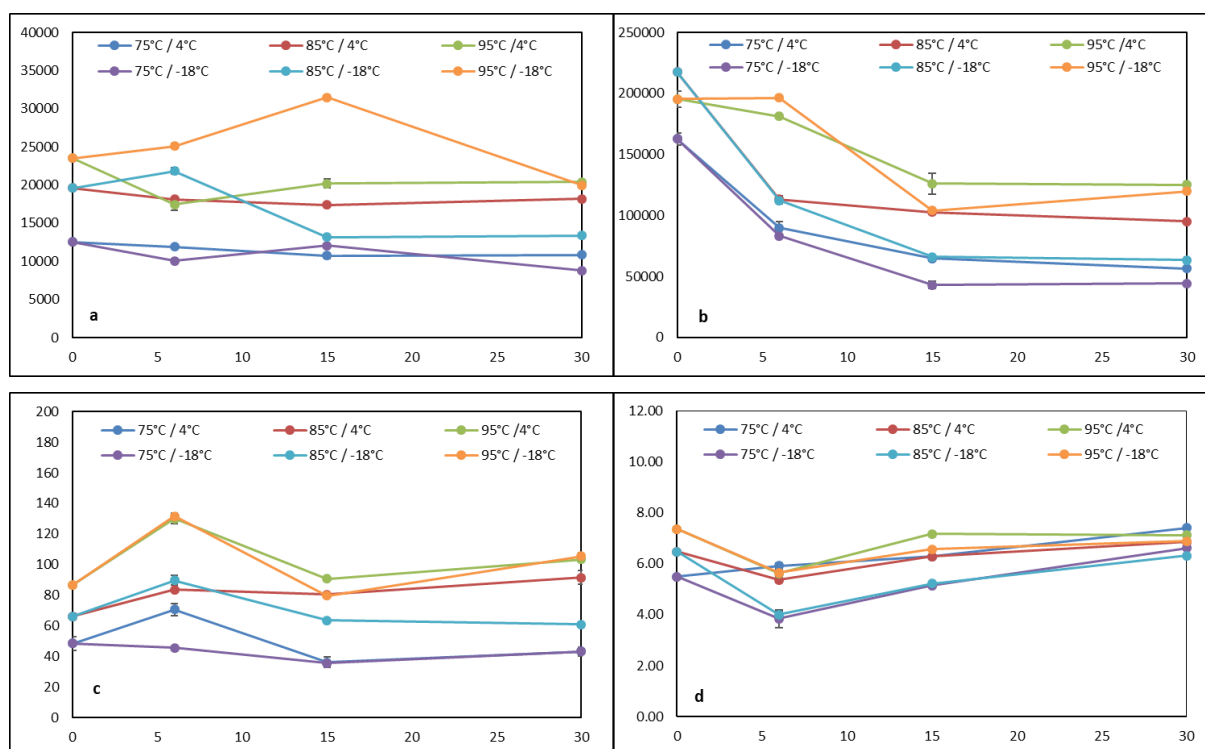


Figure 2. a) total phenolic content ($\mu\text{g GA/g}$), b) total flavonoid content ($\mu\text{g quercetin/g}$), c) free radical scavenging capacity ($\mu\text{mol trolox/g}$), and d) iron chelating capacity ($\mu\text{mol EDTA/g}$) versus storage days graphs of linden flower infusions produced at 75°C, 85°C, and 95°C and stored at (+) 4°C and (-) 18°C for 30 days. The results were calculated as dry weight basis.

3.3. Storage stability of linden leaf infusions

A significant increase in the TPC, FRSC, and ICC of linden leaf tea brewed at elevated temperature. The linden leaf tea stored +4°C and -18°C preserved their TPC between 86% and 100% at the end of 30-day storage (Figure 3). A similar observation was done for TFC of the samples stored for 30 days at + 4°C, which was between 92% and 96% of the initial TFC. TFC of linden leaf teas samples stored at -18°C decreased by approximately 50% after 30 days. Interestingly, the flavonoid contents of these teas reached their highest levels on day six of both storage conditions. While the TFC of all linden leaf teas stored +4°C increased by 12% on the 6th storage day. The antioxidant activities of these teas followed a different path from the TPC behaviors, although the phenolic content of teas decreased during storage, or the flavonoid amounts reached their highest values after 6 days and then decreased. While the FRSC of linden leaf teas stored at +4°C decreased in the first days of storage. They reached their highest FRSC value on the 15th day (except linden leaf tea brewed at 95°C and stored at -18°C). These increases were higher in teas brewed at lower temperatures. ICCs of the samples were also preserved during storage. Due to the physical and chemical properties of linden leaf tea, the increment in TPC and ICC were determined during the storage. This high stability of linden leaf tea ingredients, regardless of the brewing temperature and storage condition, indicates that linden leaf tea has the potential to be a natural additive to prevent or delay oxidation of liquid or frozen products.

In both storage conditions of linden leaf teas, pH values decreased with increasing storage time and tea samples became more acidic. While there is a slight decrease in the L^* values of tea stored at + 4 °C during the storage process, there is a slight increase in a^* values over time, while the increase in b^* values is more evident. The yellowish color of linden leaf teas that stored +4°C by time increased, which might be caused by the phenolic components that were oxidized and become dark.

3.4. Storage stability of sage leaf infusions

Unlike other tea samples, the limited increments were determined in TPC, TFC, FRSC and ICC values of sage leaf teas brewed at elevated temperatures. During the 30-day storage of sage leaf teas produced by brewing at 75,

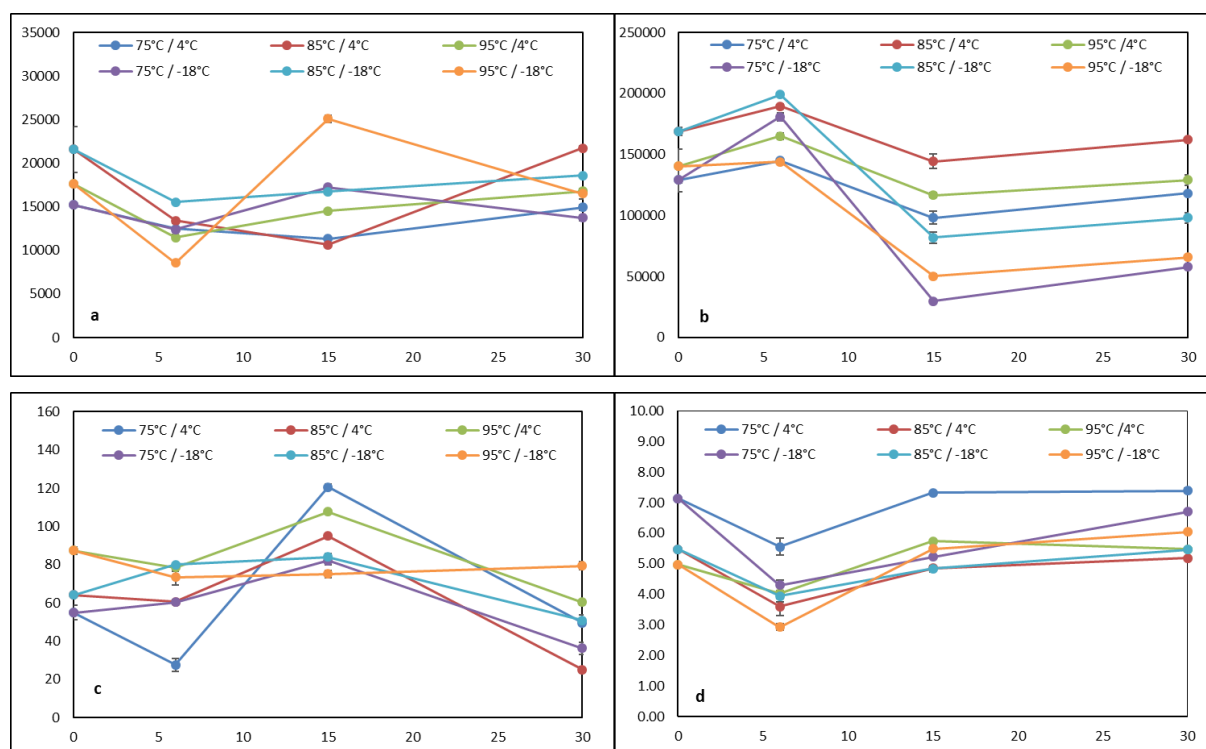


Figure 3. a) total phenolic content (µg GA/g), b) total flavonoid content (µg quercetin/g), c) free radical scavenging capacity (µmol trolox/g), and d) iron chelating capacity (µmol EDTA/g) versus storage days graphs of linden leaf infusions produced at 75°C, 85°C, and 95°C and stored at (+) 4°C and (-) 18°C for 30 days. The results were calculated as dry weight basis.

85 and 95 °C, significant changes were observed in TPC, FRSC, ICC, pH and color values of teas stored at +4 and -18 °C (Figure 4). Especially, the TPC, FRSC, and ICC of teas brewed at 75 and 85 °C were either preserved or increased up to 1.9 times at the end of 30-day storage in both studied conditions. TPC, FRSC and ICC values of teas were 12219 ± 1344 and 17830 ± 283 µg GA / g, 79 ± 5 to 104 ± 6 µmol trolox / g and 5.13 ± 0.02 to 6.81 ± 0.13 µmol EDTA / g, respectively. As a result of the storage of teas brewed at 95 °C in both conditions, TPC and FRSC values decreased from 50% to 70%, and from 30% to 40%, while ICC values remained at similar values. Chohan et al. (2008) found that the total antioxidant capacity of the sage (*Salvia fruticosa*) plant was 625 ± 0.5 µmol trolox / g in their study, in which they investigated the effect of cooking and storage processes on the antioxidant capacity of some edible plants. At the end of 30 days, a significant part of TFC of sage leaf teas stored at +4°C and at -18°C were lost, but the highest TFC values reached in the 6th day measurements of all tea samples. From the 6th to the 15th day, dramatic decreases in TFC values were obtained. In this case, it is thought that the solubility of flavonoids in tea during storage may have increased in the first days due to depolymerization, and then there may be partial decomposition in the structural integrity or solubility due to oxidation or polymerization (Alara et al. 2021).

While the pH values of sage leaf teas brewed at different temperatures decreased significantly during storage at +4 °C, they showed more limited changes during storage at -18°C. The L*, a* and b* values of teas brewed at 75°C changed very slightly in both storage conditions, while remarkable decreases in L* values and significant increases in a* values of teas brewed at 85°C and 95 °C were determined.

3.5. Storage stability of sage stem infusions

TPC and TFC contents of sage stem teas brewed at different temperatures showed significant increases when compared with the samples produced at 25°C (13-15 and 34-41-fold, respectively). No significant increase was observed in FRSC value, while ICC values increased (Figure 5). However, the teas were more acidic with a significant decrease in the pH value. According to the color measurements, the teas were darker, less reddish, and more yellowish ($P < 0.05$). The sage teas brewed at different temperatures and stored at +4°C and -18 °C for 30 days preserved their TPC value while significant increases were observed in the FRSC and ICC. TPC values of sage teas stored at +4 °C varied between 22217 ± 2362 and 23809 ± 1546 µg GA / g at the end of 30 days, while the

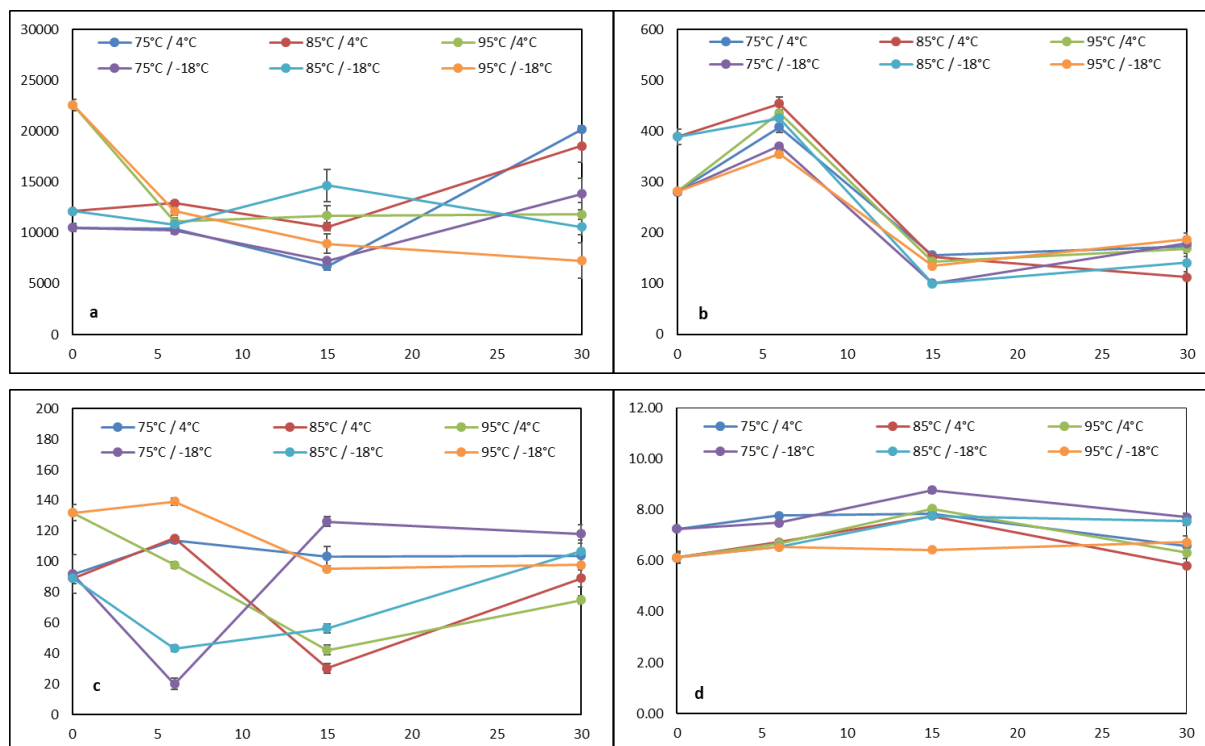


Figure 4. a) total phenolic content ($\mu\text{g GA/g}$), b) total flavonoid content ($\mu\text{g quercetin/g}$), c) free radical scavenging capacity ($\mu\text{mol trolox/g}$), and d) iron chelating capacity ($\mu\text{mol EDTA/g}$) versus storage days graphs of sage leaf infusions produced at 75°C, 85°C, and 95°C and stored at (+) 4°C and (-) 18°C for 30 days. The results were calculated as dry weight basis.

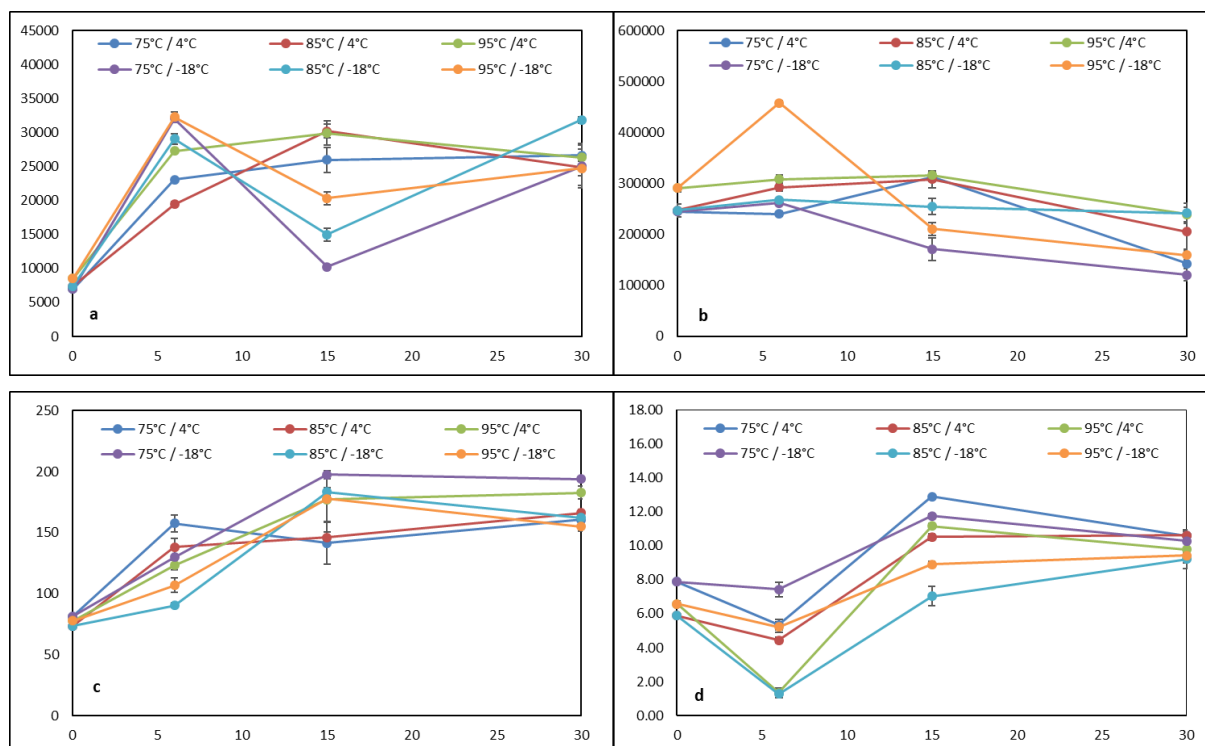


Figure 5. a) total phenolic content ($\mu\text{g GA/g}$), b) total flavonoid content ($\mu\text{g quercetin/g}$), c) free radical scavenging capacity ($\mu\text{mol trolox/g}$), and d) iron chelating capacity ($\mu\text{mol EDTA/g}$) versus storage days graphs of sage stem infusions produced at 75°C, 85°C, and 95°C and stored at (+) 4°C and (-) 18°C for 30 days. The results were calculated as dry weight basis.

values of teas stored at -18°C varied between 22086 ± 916 and 28453 ± 399 $\mu\text{g GA} / \text{g}$ during storage. Unlike the TPC values, significant decreases in TFC values were detected during storage, and these reductions were from 17% to 41% and from 2% to 51% at the end of 30 day-storage for tea samples stored at +4 and -18°C, respectively. However, the maximum TFC values were at 15th day of storage at + 4°C. It was seen that the increase in the FRSC of tea samples stored at + 4°C had a positive correlation with storage time and brewing temperature. FRSC values of sage stem teas increased approximately 2.0, 2.3 and 2.4 times for tea samples steeped at 75, 85 and 95 ° C at the end of 30 days, respectively. The increase in antioxidant activity continued and reached the maximum level at the 30th day. The FRSCs of the sage stem samples stored at -18°C reached their maximum values at the 15th day of storage and then slightly decreased.

Sage stem teas had lower pH values during storage, and it was seen that this decrease was more in teas stored at + 4 °C. While the L^* values of teas stored at -18 °C increased in 30 days of storage, no significant changes were observed in the L^* values of teas stored at + 4 °C. The b^* values of teas stored at -18 °C decreased significantly the yellowish colors of teas disappeared. When evaluated together with other results, it is thought that the lightning and yellowish color of the stored teas may be related to the soluble flavonoids found in teas.

4. Conclusions

Different herbs have been used for centuries in many different societies as a source of pharmaceuticals. Some of them also have been consumed in different ways; brewing, decoction, and infusions are the most applied ways to get benefit from them. The infusion process provides better phenolic and antioxidant extraction from the herbs and their different parts as flower, bark, stem, etc. The infusion temperature has a significant impact on the extraction yield where the higher temperature extracted higher amounts of the compounds. On the other hand, different storage temperatures changed the antioxidant and phenolic content of the infusions in similar trends. These results were interesting since the freezing was expected to preserve the phenolic compounds and antioxidant activity in infusions was better than storing them in a cooled environment. The best antioxidant preservation was observed in linden flower, linden leaf, and sage leaf infusions. However, the phenolic and antioxidant activity decreased in cinnamon infusions. This study opens a perspective to benefit from some medicinal and aromatic herbs to be used as natural antioxidant sources.

Acknowledgement

This work was supported by Adana Alparslan Türkeş Science and Technology University Scientific Research Coordination Unit. Project Number: 17103012.

Authors' Contributions

LYA: Conceptualization, Methodology, Resources, Writing - Review & Editing, Supervision, Project administration, Funding acquisition. **FGA:** Validation, Formal analysis, Investigation, Data Curation, Writing - Original Draft, Visualization.

Declaration of Ethical Standards

The author(s) of this article declare that the materials and methods used in this study do not require ethical committee permission and/or legal-special permission.

Conflict of Interest

There is no conflict of interest in this study.

References

- [1] Akcakaya F.G., Aydemir L.Y. (2019). Effects of preparation conditions on antioxidant potential of some herbal teas. *The Journal of Animal and Plant Sciences* , 29,149–157.
- [2] Fărcaș A.C., Socaci S.A., Tofană M., et al (2015). Comparative Evaluation of Biofunctional Compounds Content from Different Herbal Infusions. *Bulletin of University of Agricultural Sciences and Veterinary Medicine Cluj-Napoca Food Science and Technology*, 72, (2), 237-241.
- [3] Roby M.H.H., Sarhan M.A., Selim K.A.H., Khalel K.I. (2013). Evaluation of antioxidant activity, total phenols and phenolic compounds in thyme (*Thymus vulgaris* L.), sage (*Salvia officinalis* L.), and marjoram (*Origanum majorana* L.) extracts. *Industrial Crops and Products* , 43,827–831.
- [4] Vallverdú-Queralt A., Regueiro J., Martínez-Huélamo M., et al (2014). A comprehensive study on the phenolic profile of widely used culinary herbs and spices: Rosemary, thyme, oregano, cinnamon, cumin and bay. *Food Chemistry*, 154, 299–307.
- [5] Yoo K.M., Lee C.H., Lee H., et al (2008). Relative antioxidant and cytoprotective activities of common herbs. *Food Chemistry*,106, 929–936.
- [6] Katalinic V., Milos M., Kulisic T., Jukic M. (2006). Screening of 70 medicinal plant extracts for antioxidant capacity and total phenols. *Food Chemistry*, 94, 550–557.
- [7] Islam M.Z., Cho D.K., Lee Y.T. (2020). Bioactive compounds and antioxidant capacity of tea infusion prepared from whole and ground medicinal herb parts. *CYTA - Journal of Food*, 18, 116–121.
- [8] Martins N., Barros L., Santos-Buelga C., et al (2014). Evaluation of bioactive properties and phenolic compounds in different extracts prepared from *Salvia officinalis* L. *Food Chemistry*, 70, 378–385.
- [9] Olszowy M. (2019). What is responsible for antioxidant properties of polyphenolic compounds from plants? *Plant Physiology and Biochemistry*, 144, 135–143.
- [10] Apel K., Hirt H. (2004). Reactive oxygen species: Metabolism, oxidative stress, and signal transduction. *The Annual Review of Plant Biology* , 55, 373–399.
- [11] Halliwell B. (1996). Commentary Oxidative Stress, Nutrition and Health. *Experimental Strategies for Optimization of Nutritional Antioxidant Intake in Humans. Free Radicals Research*, 25, 57–74.
- [12] Wahid A., Gelani S., Ashraf M., Foolad M.R. (2007). Heat tolerance in plants: An overview. *Environmental and Experimental Botany*, 61, 199–223.
- [13] Dvorackova E., Snoblova M., Chromcova L., Hrdlicka P. (2015). Effects of extraction methods on the phenolic compounds contents and antioxidant capacities of cinnamon extracts. *Food Science and Biotechnology*, 24, 1201–1207.
- [14] Park J.B. (2011). Identification and quantification of a major anti-oxidant and anti-inflammatory phenolic compound found in basil, lemon thyme, mint, oregano, rosemary, sage, and thyme. *International Journal of Food Science and Nutrition* , 62, 577–584.
- [15] Şanlı S., Lunte C. (2014). Determination of eleven flavonoids in chamomile and linden extracts by capillary electrophoresis. *Analytical Methods*, 6, 3858–3864.
- [16] Sroka Z., Belz J. (2009). Antioxidant Activity of Hydrolyzed and Non – Hydrolyzed Extracts of the Inflorescence of Linden (*Tiliae inflorescentia*) * Aktywność przeciwutleniająca hydrolizowanych i niehydrolizowanych. *Advances in Clinical and Experimental Medicine* , 18, 329–335.
- [17] Singleton V.L., Rossi J.A. (1965). Colorimetry of total phenolics with phosphomolybdic-phosphotungstic acid reagents. *The American Journal of Enology and Viticulture* , 16, 144–158.
- [18] Zhishen J., Mengcheng T., Jianming W. (1999). The determination of flavonoid contents in mulberry and their scavenging effects on superoxide radicals. *Food Chemistry*, 64, 555–559.
- [19] Sanchez-Moreno C., Larrauri J.A., Saura-calixto F. (1998). A Procedure to Measure the Antiradical Efficiency of Polyphenols. *Journal of the Science of Food and Agriculture* , 270, 270–276.
- [20] Aydemir L.Y., Gökbulut A.A., Baran Y., Yemenicioğlu A. (2014). Bioactive, functional and edible film-forming properties of isolated hazelnut (*Corylus avellana* L.) meal proteins. *Food Hydrocolloids*, 36,130–142.